UNPUBLISHED PRELIMINARY DATA

FINAL REPORT

on Grant No. NsG 221-62

NATIONAL AERONAUTICS AND SPACE ADMINISTRATION

A LOG PERIODIC MONOPOLE ANTENNA

by

Clayton Clark

G. Paul Francis

Ming-hui Chen

July 20, 1964

OTS PRICE

$ 3.60 ph $

XEROX MICROFILM

FACILITY FORM 602

N64-29701 (ACCESSION NUMBER) 96 (PAGES) CR 58628 (NASA CR OR TMX OR AD NUMBER)

N64-29703 (THRU) 1 (CODE) 08 (CATEGORY)

ANTENNA AND PROPAGATION LABORATORY
Department of Electrical Engineering
Engineering Experiment Station
UTAH STATE UNIVERSITY
Logan, Utah

REPORTS CONTROL No. 1

FINAL REPORT

on Grant No. NsG 221-62

NATIONAL AERONAUTICS AND SPACE ADMINISTRATION

A LOG PERIODIC MONOPOLE ANTENNA

by

Clayton Clark
G. Paul Francis
Ming-hui Chen

July 20, 1964

ANTENNA AND PROPAGATION LABORATORY
Department of Electrical Engineering
Engineering Experiment Station
UTAH STATE UNIVERSITY
Logan, Utah

TABLE OF CONTENTS

INTRODUCTION

This is the final report on National Aeronautics and Space Administration Grant No. NsG 221-62. This grant has supported a study of the log-periodic principle applied to a "monopole" antenna. 29702

The "monopole" as used in this study, consists of a single "toothed" structure mounted above a reflecting sheet. The driving terminals are the tip of the monopole and the reflecting sheet. The monopole has been mounted in a number of ways including flush mounting over an air filled cavity and over a dielectric filled cavity. The performance of the structure has been calculated and measured for each mounting arrangement over a frequency range of 2 Gc to 4 Gc. Results are summarized below.

Some details of measurements and computations have been reported previously as noted below. Other computations and comparison of calculated results with measured performance are shown in Appendices A and B in this final report.

HISTORY OF THE PROJECT

Some preliminary work by Clark and Brownell [1] and Clark and Johnson [2] resulted in a proposal to NASA for a research grant to develop the log periodic monopole antenna. NASA Grant No. NsG 221-62 became effective 12 February 1962 in the amount of $17,000 for a two year program.

Work has progressed uniformly and has led to Master's Degree thesis material for four students: Allen Leigh, Richard L. Whale, G. Paul Francis, and Ming-hui Chen. Their work was reported in thesis form and was then included as the major content of Interim Reports 1 and 2 and this Final Report.

The termination date of the original grant was extended to 30 June 1964 to permit utilization of the school year for completion of the study. Extension was authorized by Dr. T.L.K. Smull in a letter dated 21 August 1963.

On May 1, 1964, a paper entitled "A Flush Mounted Log Periodic Antenna" was presented by G. Paul Francis and Clayton Clark in the Antenna and Propagation Session of the IEEE Region 6 Annual Conference in Salt Lake City. This paper summarized the development of the monopole antenna and presented the results of measurements of performance in air and in a dielectric filled cavity.

SUMMARY OF RESULTS

This work has involved a theoretical and experimental investigation of a monopole antenna protruding from a ground plane. Descriptions and illustrations of the device and the test configurations are included in previous reports and in the appendices to this final report. For an example see page 9 of Appendix A. The results obtained by each worker or each separate team is summarized below with references to the complete reports containing the detailed work of each.

Interim Report (No. 1) - Clark, Jones and Leigh [3]

This first interim report carried no number since it was anticipated at the time that the next report would be a final report. The parentheses used above indicate that the number 1 did not appear on the report.

An experimental study was carried out by Mr. Leigh. His complete Master's Degree thesis reporting his findings is bound with the Interim Report as Appendix A. Some preliminary theoretical work by Clark and Jones was also included.

The results are summarized as follows:

(1) The log periodic monopole structure was found to exhibit the broadband characteristics typical of other log periodic antennas. The radiation pattern followed predictions based on the number of active elements and remained the same shape and the same position relative to the ground plane at any frequency within the design range. The driving point impedance was constant within a factor of approximately 2 over the design frequency range.

(2) To minimize variations of pattern and impedance with frequency changes it was necessary to mount the monopole at an angle of approximately 15 degrees with the ground plane. At this angle, the separation between an active element on the log periodic monopole and its image in the ground plane remains near a half wavelength for any frequency.

(3) It was found to be permissible to recess the ground plane structure near the monopole antenna so that the monopole lay in the plane of the surrounding ground plane provided the angle of 15 degrees was maintained between the monopole and the floor of the recessed cavity. Frequency independent characteristics were not impaired provided the cavity edges were not closer than approximately an eight wavelength from the longest element of the antenna. Effects of variations in cavity size and shape were reported.

Interim Report No. 2 - Whale and Clark [4]

This work was performed largely by Mr. Whale under the direction of Dr. Clark. An equation was written to describe theoretically the log periodic monopole pattern when operating over a ground plane. The method of images was used. The equation was evaluated by hand computations for only a few points to show comparison with measurements. The effects of dielectric material in the recessed cavity were studied experimentally. The results of this study may be summarized as follows:

(1) The method of images yielded an equation which describes with reasonable accuracy the radiation pattern in the H plane of the log periodic monopole antenna over a reflecting sheet.

(2) The cavity under a flush mounted log periodic monopole was filled with low-loss dielectric material without sacrifice of the broadband pattern characteristics provided dimensions and angles were adjusted to permit the same phase relationships as in air. A miniaturized antenna was achieved.

(3) The driving point impedance was altered by the dielectric so that higher standing wave ratios were noted. Further study of this aspect is needed.

Theoretical Work by Francis, Chen and Clark

Enclosed as appendices are reports prepared by G. Paul Francis and Ming-hui Chen. Both have used a computer to determine pattern shapes using the method of images.

Mr. Francis calculated the performance of the monopole in air and rechecked the experimental results to verify the performance comparison. Appendix A of this report shows the work in detail. Appendix A has listed also some results of an optimization study by Mr. Francis.

Mr. Chen in Appendix B, derived an equation to describe the three-dimensional radiation pattern in air produced by the log periodic monopole immersed in a dielectric. The final equation shown on page 19 of Appendix B is very complex, as would be expected. The results in the H plane are plotted on page 20 and indicate that the basic variables are included in the equation but it still does not completely describe the performance. Agreement between theory and measurement is perhaps as close as could be expected in a structure so complicated.

CONCLUSIONS

A new type of antenna was developed with the support of the subject research grant. It is a practical design with broadband characteristics and gain which may be set as desired in the design.

The work was originally an engineering experimental development but this was later supported by a computer programmed analysis.

Immersion of the monopole in a low-loss dielectric within a recessed cavity was shown to be a satisfactory method of producing a miniaturized flush-mounted antenna.

Further work is needed to determine the impedance characteristics and optimum methods of feeding the monopole antenna when it is mounted in a dielectric filled cavity.

LITERATURE CITED

1. Clark, C. and F.P. Brownell, Status Report to 1 March 1962, Diamond Ordnance Fuze Laboratory Project No. DA-49-186-502-ORD-769, "VHF and UFH Excitation of Various Geometric Shapes."

2. Clark, C. and R.J. Johnson, Final Report, Diamond Ordnance Fuze Laboratory Project No. DA-49-186-502-ORD-769, 30 June 1961 "VHF and UFH Excitation of Various Geometric Shapes,"

3. Clark, C., W.L. Jones, and A. Leigh, Interim Report (No. 1) on Research Grant No. NsG 221-62, NASA, "A Theoretical and Experimental Investigation of Flush Mounting Configurations for Log Periodic Structures."

4. Whale, R.L., C. Clark, Interim Report No. 2 on Research Grant No. NsG 221-62, NASA, "A Log Periodic Monopole Antenna in a Dielectric Filled Cavity."

5. Francis, G. P., Master's Thesis, USU, EE Department, 1964, "Analysis of a Cavity-Mounted Log-Periodic Monopole Antenna."

6. Chen, M., Master's Thesis, USU, EE Department, 1964, "The Radiation Patterns of a Log Periodic Monopole Antenna."

N64-29702

APPENDIX A

ANALYSIS OF A CAVITY-MOUNTED LOG-PERIODIC MONOPOLE ANTENNA

by

G. Paul Francis

ACKNOWLEDGMENTS

The author wishes to express his thanks to those who have helped in the research and especially in the preparation of this report, Dr. Clayton Clark and Ming-hui Chen.

This work was sponsored by the National Aeronautics and Space Administration under Research Grant No. NsG-221-62.

G. Paul Francis

TABLE OF CONTENTS

LIST OF TABLES

LIST OF FIGURES

INTRODUCTION

The flush-mounted log-periodic antenna exhibits electrical characteristics which are essentially independent of frequency over a given bandwidth. This bandwidth is limited, theoretically, only by the practicality of physical size of the antenna at the low frequency end and feeding problems at the high frequency end.

ABST 29702

This report covers the investigation (primarily by digital computer techniques) of the H-plane radiation pattern of the antenna when mounted over a cavity. Information is also given on the E-plane patterns and the driving point impedance.

This work has five objectives:

(1) To design an antenna which will have uniform radiation patterns over a wide frequency band;

(2) To design an antenna which will have essentially constant input impedance over the same wide frequency band;

(3) To illustrate the basic design of a flush-mounted log-periodic monopole-tooth antenna;

(4) To present a computer solution of the basic H-plane radiation pattern equation for the antenna mounted over an air-filled cavity;

(5) To provide information for optimizing the antenna design.

Author

An equation for the H-plane radiation pattern was written by Whale

and Clark (1963). Some modifications were made in the equation and a computer program was written to utilize the IBM 1620 computer in solving it. The results from the computer are compared with air-cavity pattern measurements. Two antenna design parameters (the logarithmic ratio τ and the cavity-floor angle γ) were varied and the computer program was used in obtaining information for their optimization.

Measured E-plane radiation patterns and normalized input impedance characteristics are presented.

HISTORY

The log-periodic antenna concept was first proposed by DuHamel and Isbell in 1957. Their antenna had solid teeth which were spaced non-uniformly with a linear taper along one or more center conductors. They referred to their antenna as log-periodic, because the impedance properties repeated periodically with the logarithm of the frequency.

DuHamel and Ore (1958) developed a triangular-tooth structure and then replaced the solid teeth with wire outlines (see Figure 1) and found that this structure performed equally well as the solid-tooth structure.

Isbell (1960) made the next major step when he replaced the wire outlines by a sequence of parallel dipoles, with single thin linear elements approximating the wire-outline triangular-tooth structures shown in Figure 1.

One half of the log-periodic array studied by Isbell was used in this study. It is referred to as a log-periodic monopole antenna.

Brownell (1961) studied the log-periodic monopole antenna mounted at various angles over a ground plane and verified that the structure still maintained its log-periodic characteristics.

Clark, Jones and Leigh (1962) investigated the log-periodic monopole antenna mounted over a recessed cavity and reported on the effect of

varying the cavity parameters on the radiation patterns and on the driving-point impedance.

Whale and Clark (1963) derived a basic H-plane radiation pattern equation for the monopole-tooth antenna mounted above an air-filled cavity and experimentally studied the effects of mounting the antenna in a dielectric filled cavity.

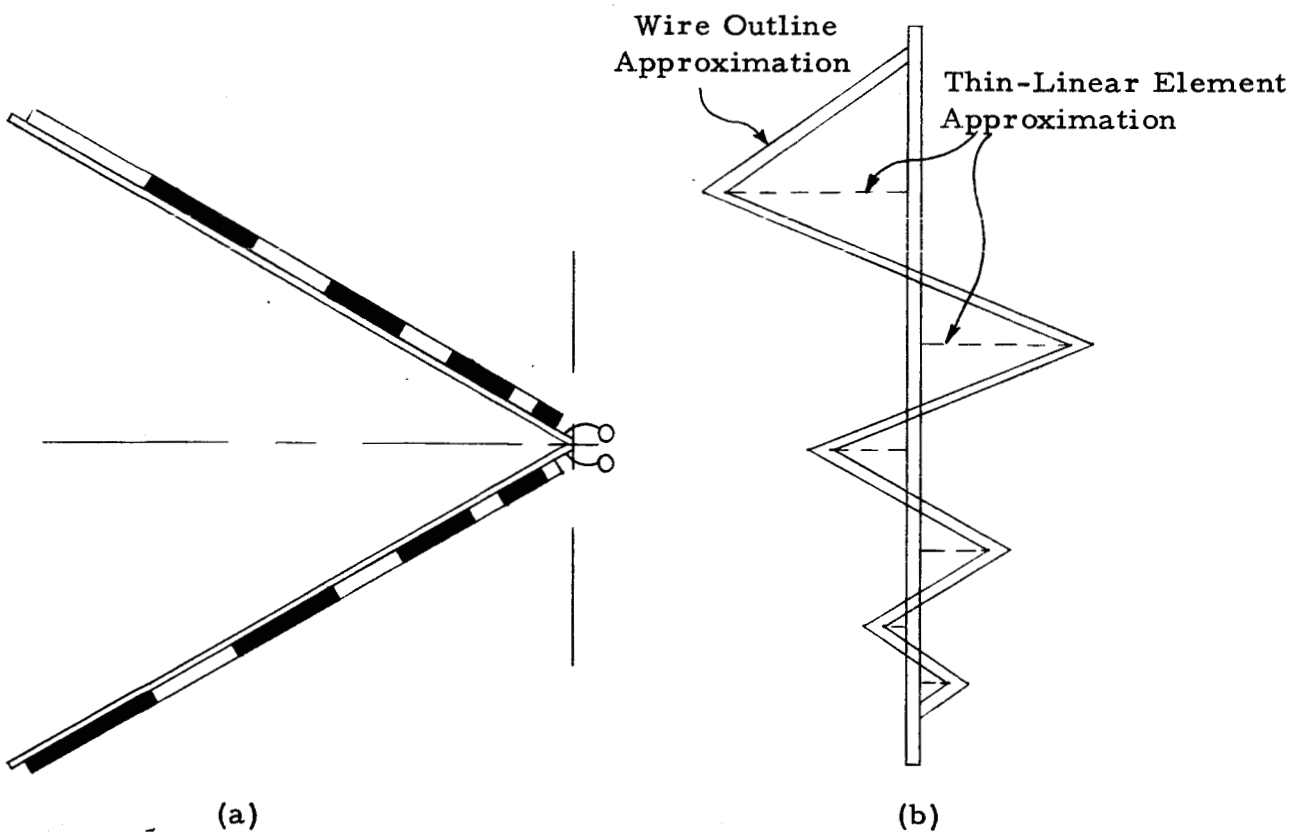

Figure 1. Parameters for triangular-tooth antenna. (a) Side view, (b) Plan view of one-half of antenna.

THEORY

To design a log-periodic monopole antenna with tooth-type elements, certain parameters, characteristic angles and lengths must be defined. These are illustrated in Figure 2. The angle α defines the taper of the antenna and is defined as

$$\alpha = \tan^{-1} \frac{L_N}{S_N} \tag{1}$$

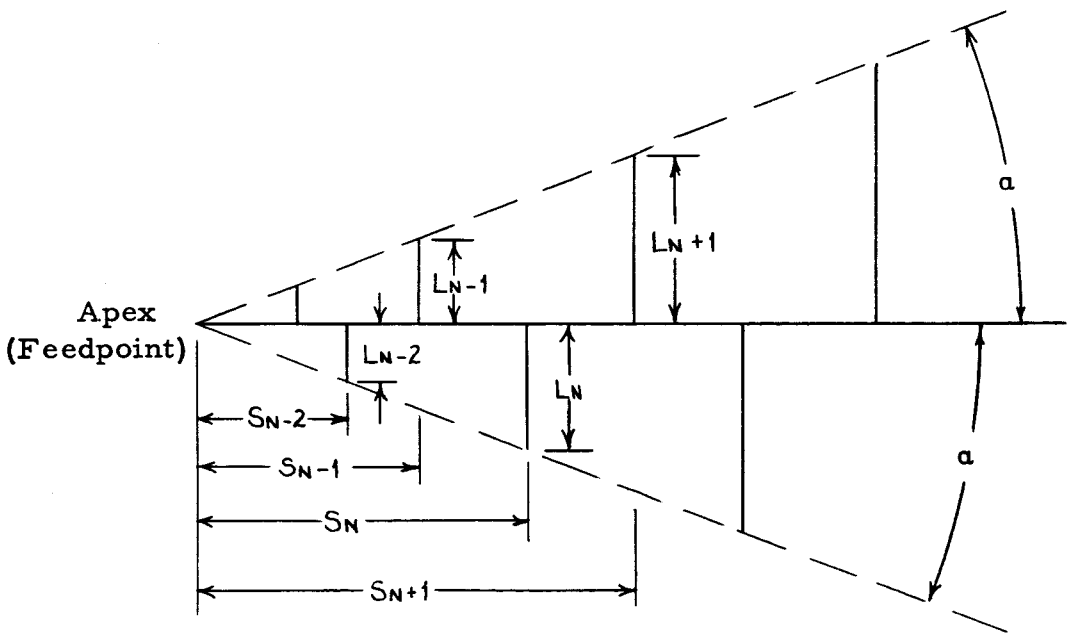

Figure 2, Characteristic dimensions of a log-periodic monopole antenna with tooth-type elements.

The logarithmic ratio τ is the ratio of two similar dimensions of the antenna and is always less than unity. For this report, τ is defined as

$$\tau = \frac{L_{N-1}}{L_N} = \frac{S_{N-1}}{S_N} \tag{2}$$

where L_N and S_N are defined in Figure 2, and N is the number of a general tooth.

Another specification for the antenna design is the desired frequency range of operation. Thus, the highest frequency of operation establishes the length (approximately $\lambda/4$) of the shortest element and the lowest frequency of operation establishes the length of the longest element.

The length of any element of order N is given by $\tau^N L$, where L is the length of the longest element. The spacing from the apex to any element of order N is given by $\tau^N S$ where S is the distance from the apex to the longest element.

Those elements which radiate the major part of the energy will be those which are closest to resonance ($\lambda/4$) at the operating frequency. This leads to the fact that any array has three-to-five active-elements as discussed by Bell, Elfving, and Franks (1960). They found that almost all power radiated by the antenna is radiated from this active-element array. The number of elements to be chosen for the active array

increases as τ approaches unity. In our case a value of τ (0.85) was chosen which indicated that a choice of 4 active elements would be reasonable. As the excitation frequency is changed, the position of the active element array also changes. In essence this is what causes the antenna to be frequency independent. It is, however, desirable to have this transition from one active array to another as smooth as possible. This is controlled by τ. The elements which are longer than the elements radiating power act as reflectors, and the elements shorter than the elements radiating power act as directors.

Since the antenna is an unbalanced structure, it is fed against a ground plane as shown in Figure 3. Mounting the antenna above a ground-plane cavity of angle γ causes "mirror images" of the active elements to be formed on a line at an angle γ below the floor of the cavity. Figure 4 shows a typical H-plane radiation pattern for the cavity mounted log-periodic antenna.

Isbell (1960) has shown that the currents alternate down the active elements in the antenna (as seen in Figure 3).

The radian distance (phase shift due to this distance) perpendicular from the cavity floor to the resonant element (dr) is given by

$$dr = (2\pi) \tan \gamma \qquad (3)$$

radians.

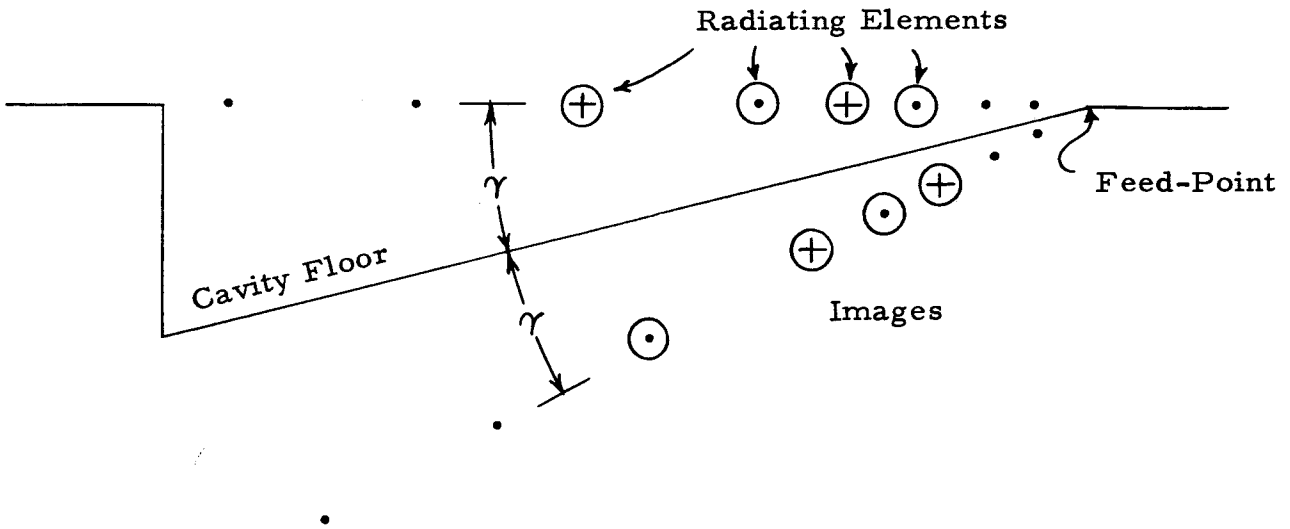

Figure 3. Log-periodic monopole antenna radiating elements. Shown is the side view of the antenna with its "mirror images."

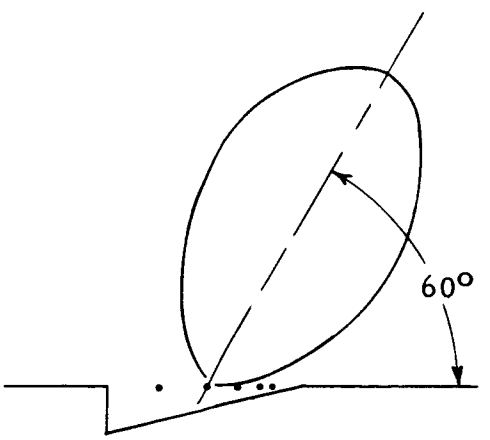

Figure 4. Typical H-plane radiation pattern orientation.

This is based on the assumption that the distance from the apex to the resonant element is one wavelength. This will be more fully explained in the next section.

The phase shift dr_1 in the wave as it travels from element L_N to element L_{N+1} is

$$\frac{2\pi}{\lambda}[S_{N+1} - S_N] = \frac{2\pi}{\lambda}[\lambda_{N+1} - \lambda_N] = \frac{2\pi}{\lambda}\left[\frac{C}{f_{N+1}} - \frac{C}{f_N}\right] = \frac{2\pi C}{\lambda}\left[\frac{1}{\tau f_N} - \frac{1}{f_N}\right]$$

$$= 2\pi\left[\frac{1}{\tau} - 1\right] \qquad (4)$$

radians.

The corresponding distance between the active elements and the ground plane are expressed as shown in Figure 5.

The cosine law is used in computing the relative distances which refer the phase shifts of the images to the resonant element L_N. Figure 6 shows the definitions of the following phase shifts.

The radian distances are given as:

$$dr_2 = 2\pi\,(1 - \tau)$$

$$dr_1 = 2\pi\,(\frac{1}{\tau} - 1)$$

$$dr_7 = 2[\,dr - 2\pi\,(1 - \tau)\sin\gamma] = 2[\,dr - dr_2\sin\gamma]$$

$$dr_o = 2dr$$

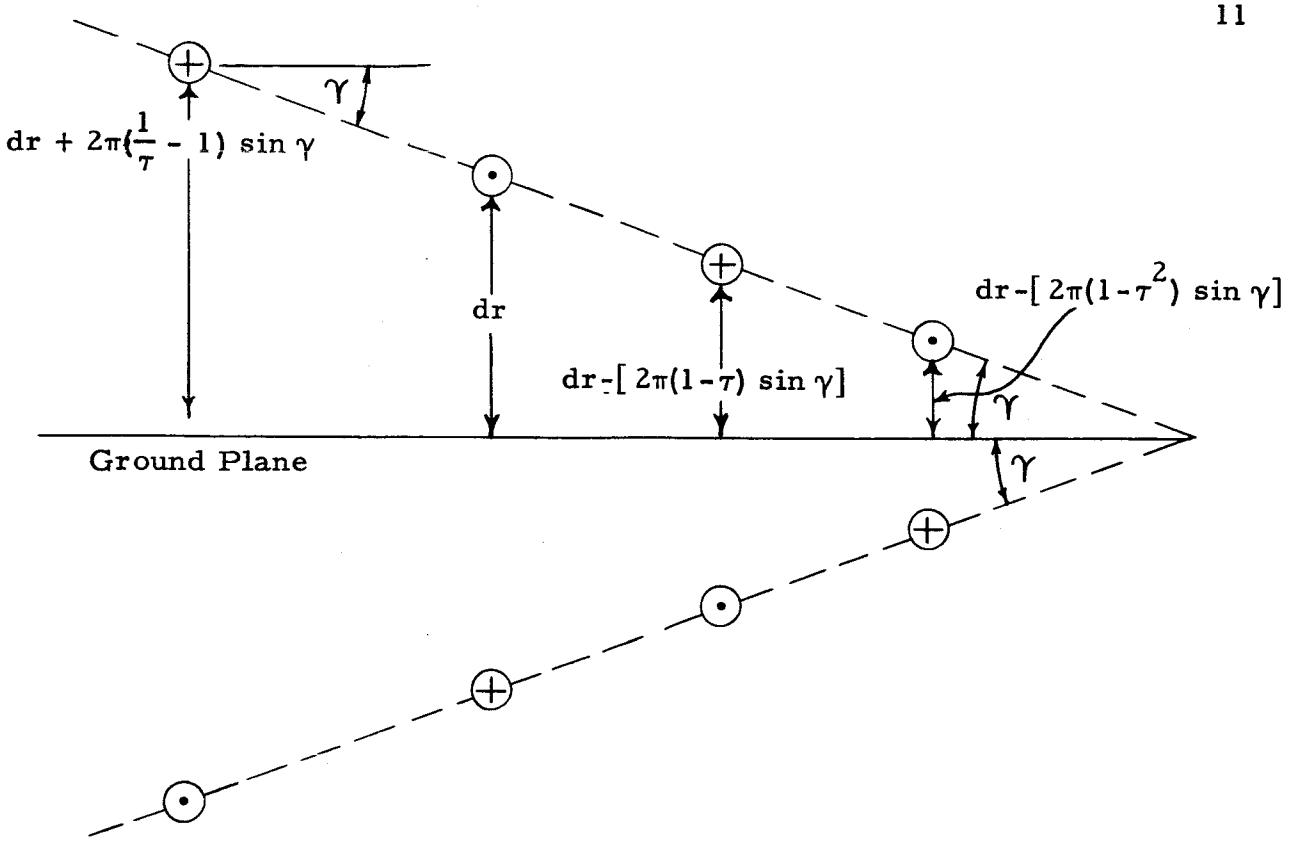

Figure 5. The phase distances between the active elements and the ground plane. The distance dr is the perpendicular distance from the resonant element L_N to the ground plane. γ is the angle the antenna plane makes with the ground plane (the cavity-floor angle).

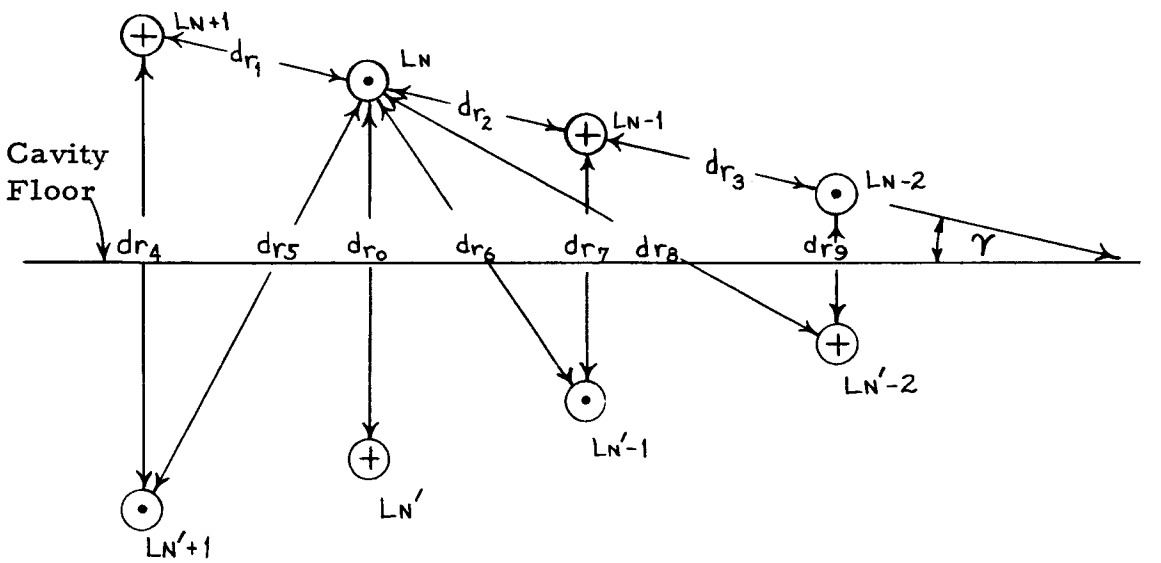

Figure 6. Specification of distances between elements. The distances are in radians of phase shift from the active elements and images to the resonant element L_N.

$$dr_4 = 2[\,dr + 2\pi\,(\frac{1}{\tau} - 1)\,\sin\gamma\,] = 2[\,dr + dr_1\,\sin\gamma\,]$$

$$dr_5 = \{4[\,dr + 2\pi(\frac{1}{\tau} - 1)\,\sin\gamma\,]^2 + [\,2\pi\,(\frac{1}{\tau} - 1)\,]^2$$

$$- 4[\,dr + 2\pi(\frac{1}{\tau} - 1)\,\sin\gamma\,]\;2\pi(\frac{1}{\tau} - 1)\,\cos\,(90^\circ - \gamma)\}^{\frac{1}{2}}$$

$$= [\,dr_4^{\,2} + dr_1^{\,2} - 2dr_4 dr_1\,\cos\,(90^\circ - \gamma)\,]^{\frac{1}{2}}$$

$$dr_{10} = dr_2 + dr_3 = 2\pi(1 - \tau^2)$$

$$dr_9 = 2[\,dr - 2\pi\,(1 - \tau^2)\,\sin\gamma\,] = 2[\,dr - dr_{10}\,\sin\gamma\,]$$

$$dr_8 = \{4[\,dr - 2\pi(1 - \tau^2)\,\sin\gamma\,]^2 + [\,2\pi(1 - \tau^2)\,]^2 - 8\pi[\,dr - 2\pi(1 - \tau^2)\,\sin\gamma\,]$$

$$(1 - \tau^2)\,\cos\,(90^\circ + \gamma)\}^{\frac{1}{2}}$$

$$= [\,dr_9^{\,2} + dr_{10}^{\,2} - 2dr_9 dr_{10}\,\cos\,(90^\circ + \gamma)\,]^{\frac{1}{2}}$$

$$dr_6 = \{4[\,dr - 2\pi(1 - \tau)\,\sin\gamma\,]^2 + [\,2\pi(1 - \tau)\,]^2$$

$$- 8\pi(1 - \tau)[\,dr - 2\pi(1 - \tau)\sin\gamma\,]\,\cos\,(90^\circ + \gamma)\}^{\frac{1}{2}}$$

$$= [\,dr_7^{\,2} + dr_2^{\,2} - 2dr_2 dr_7\,\cos\,(90^\circ + \gamma)\,]^{\frac{1}{2}} \qquad (5)$$

The radiation pattern is the summation of the contributions from all the radiating elements and their mirror images. Referring to Figure 7, the radiation equation may be expressed as

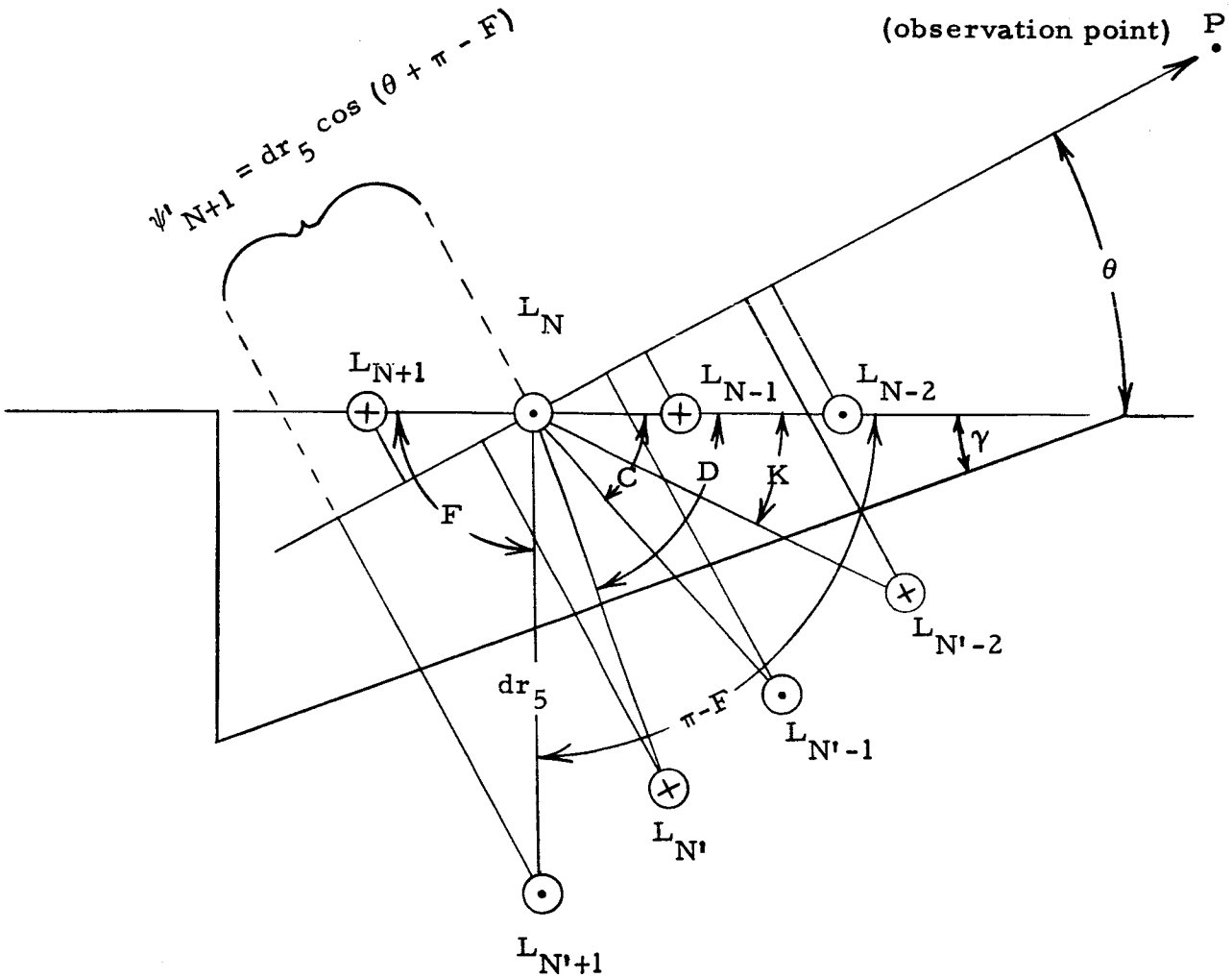

Figure 7. The relative phase shifts of the sources as a function of θ. The phase shifts are measured with respect to the reference point $L_{N'}$. These phase differences are calculated from the travel distances from each element or image to an observation point P.

$$E_T = E_{n-2}\, e^{j\,\psi_{n-2}} - E_{n-2} e^{j\,\psi'_{n-2}} - E_{n-1}\, e^{j\,\psi_{n-1}} + E_{n-1}\, e^{j\,\psi'_{n-1}} + E_n e^{j\,\psi_n}$$
$$- E_n\, e^{j\,\psi'_n} - E_{n+1}\, e^{-j\,\psi_{n+1}} + E_{n+1}\, e^{j\,\psi'_{n+1}} \qquad (6)$$

where E_n is the magnitude of the electric field contributed by element L_n.

The exponential functions, ψ_n's are:

$$\psi_{n-2} = dr_{10} \cos\theta$$

$$\psi'_{n-2} = dr_8 \cos(K + \theta)$$

$$\psi_{n-1} = dr_2 \cos\theta$$

$$\psi'_{n-1} = dr_6 \cos(C + \theta)$$

$$\psi_n = 0$$

$$\psi'_n = dr_o \cos(D + \theta)$$

$$\psi_{n+1} = -dr_1 \cos\theta$$

$$\psi'_{n+1} = dr_5 \cos(\theta + \pi - F) \qquad (7)$$

where angles K, C, D, and F are expressed as:

$$K = \cos^{-1} \frac{(dr_{10})^2 + (dr_8)^2 - (dr_9)^2}{2\,(dr_{10})\,(dr_8)}$$

$$C = \cos^{-1} \frac{(dr_2)^2 + (dr_6)^2 - (dr_7)^2}{2\,(dr_2)\,(dr_6)}$$

$$D = 90^{\circ} - \gamma \qquad (8)$$

$$F = \cos^{-1} \frac{(dr_1)^2 + (dr_5)^2 - (dr_4)^2}{2\,(dr_1)\,(dr_5)}$$

The evaluation of E_T from Equation (6) requires further information (the contribution to the field from each active element). A relation between the impedance of each monopole element and the contribution of these monopoles to the radiation field may be developed as follows:

$$E_n \text{ radiated} = k\,I_n = \frac{V_n}{Z_n} \qquad (9)$$

where E_n = the contribution to the field from the element L_n

I_n = current at the base of element L_n

V_n = voltage at base of element L_n

Z_n = base impedance of L_n (the impedance of a monopole mounted above an infinite conducting plane)

k = proportionality constant

Similar expressions may be stated for E_{n+1}, E_{n-1}, and E_{n-2}. By

normalizing each of the expressions to E_n, the resulting expressions are:

$$\frac{E_n}{E_n} = 1$$

$$\frac{E_{n-1}}{E_n} = \frac{V_{n-1}(Z_n)}{V_n(Z_{n-1})} = \frac{|V_{n-1}| \angle\delta_{n-1}(Z_n)}{|V_n| \quad \angle 0\ (Z_{n-1})}$$

$$\frac{E_{n-2}}{E_n} = \frac{V_{n-2}(Z_n)}{V_n(Z_{n-2})} = \frac{|V_{n-2}| \angle\delta_{n-2}(Z_n)}{|V_n| \quad \angle 0\ (Z_{n+2})}$$

$$\frac{E_{n+1}}{E_n} = \frac{V_{n+1}(Z_n)}{V_n(Z_{n+1})} = \frac{|V_{n+1}| \angle\delta_{n+1}(Z_n)}{|V_n| \quad \angle 0\ (Z_{n+1})} \qquad (10)$$

where δ_{n-2}, δ_{n-1}, δ_{n+1} are the voltage phases with respect to the voltage V_n.

It seems proper, as suggested by the near field measurements of Bell, Elfving and Franks (1960), that each element of the antenna be considered as a separate monopole antenna, and the center rod as a transmission line "feeding" the element.

In this first order solution for the H-plane radiation pattern equation, the mutual impedances have been neglected. It was also assumed in this derivation that the voltage wave, feeding the active region, remained constant in magnitude but varied in phase over this region.

Thus, $\left|V_{n+1}\right| = \left|V_n\right| = \left|V_{n-1}\right| = \left|V_{n-2}\right|$ and Equations (10) are expressed as:

$$\frac{E_n}{E_n} = 1$$

$$\frac{E_{n-1}}{E_n} = \frac{Z_n}{Z_{n-1}} \frac{\angle\delta_{n-1}}{\angle 0}$$

$$\frac{E_{n-2}}{E_n} = \frac{Z_n}{Z_{n-2}} \frac{\angle\delta_{n-2}}{\angle 0}$$

$$\frac{E_{n+1}}{E_n} = \frac{Z_n}{Z_{n+1}} \frac{\angle\delta_{n+1}}{\angle 0} \qquad (11)$$

where Z_n is the base impedance of element L_n

Z_{n-1} is the base impedance of element L_{n-1}

δ_{n-2} is the relative voltage phase of V_{n-2} with respect to V_n

Equation (6) is now expressed, in normalized form, as

$$\frac{E_T}{E_n} = \frac{Z_n}{Z_{n-2}} \left[e^{j(\psi_{n-2} + \delta_{n-2})} - e^{j(\psi'_{n-2} + \delta_{n-2})}\right]$$
$$- \frac{Z_n}{Z_{n-1}} \left[e^{j(\psi_{n-1} + \delta_{n-1})} - e^{j(\psi'_{n-1} + \delta_{n-1})}\right] + \left[e^{j\psi_n} - e^{j\psi'_n}\right]$$
$$- \frac{Z_n}{Z_{n+1}} \left[e^{j(\psi_{n+1} + \delta_{n+1})} - e^{j(\psi'_{n+1} + \delta_{n+1})}\right] \qquad (12)$$

This is the basic normalized H-plane radiation pattern equation for the antenna mounted above an air-filled cavity. It assumes a four-active-element array and is expressed as the sum of the fields produced by the active elements and their images, taking into account travel phase, distance, feeding phase and element impedances.

EXPERIMENTATION

Procedure

The log-periodic monopole-tooth antenna used in this experiment is shown in Figure 8. It was designed to have an upper cutoff frequency of approximately 4.0 Gc and a lower cutoff frequency of approximately 2.0 Gc. The distance from the apex to the resonant element was chosen (for measurement convenience) to be λ_N, the resonant wavelength. The design was completed by setting the length of the longest and shortest teeth at 0.25 λ where λ is the wavelength at 2.0 Gc and 4.0 Gc respectively. Because S_N is one wavelength, the antenna's taper angle is fixed ($L_N = .25\ \lambda_N$) since

$$\alpha = \tan^{-1} \frac{L_N}{S_N} = \tan^{-1} \frac{.25\ \lambda_N}{\lambda_N} = \tan^{-1} .25 = 14^o$$

The logarithmic ratio τ was chosen to be 0.85. This determined the spacing between adjacent similar antenna dimensions.

The teeth of this antenna were constructed from No. 14 copper wire soldered to a single center conductor of the same size. The ground plane was constructed of sheet brass. The dimensions were sufficient to allow it to be at least one wavelength in all directions (measured from

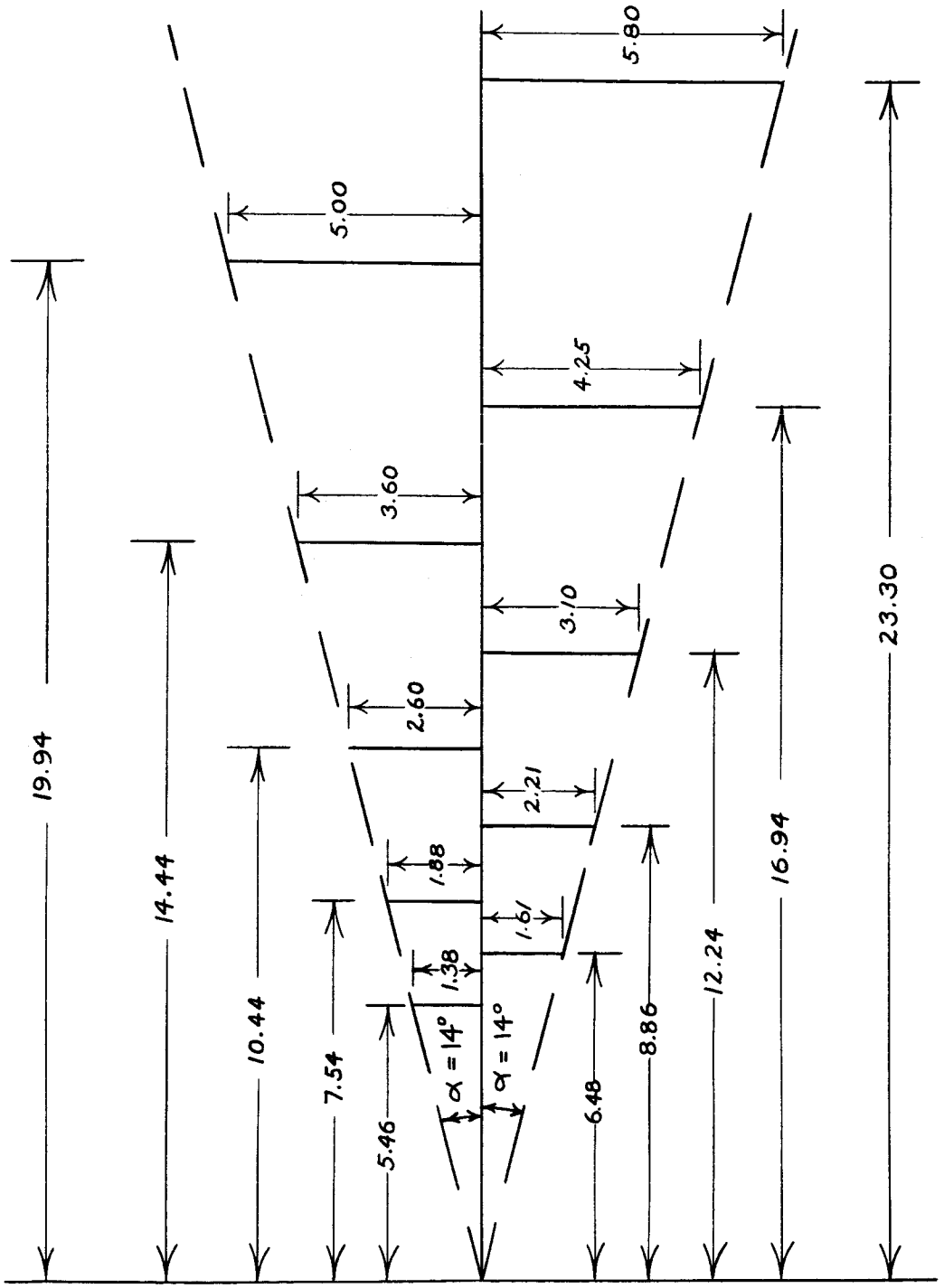

Figure 8. Dimensions of log-periodic monopole antenna mounted over an air-filled cavity. Antenna designed with $\alpha = 14^{\circ}$, $\tau = 0.85$, and frequency range 2.0 Gc to 4.0 Gc. Dimensions shown in cm.

the center of the cavity) at the lowest operating frequency. The ground plane and cavity dimensions are shown in Figure 9. From this antenna the radiation field patterns for the E- and H-planes and the driving-point impedance were measured.

A standard antenna range using the superheterodyne detection system shown in Figure 10 was used for obtaining the radiation field patterns. The coordinate system shown in Figure 12 was used. The driving point impedance was measured on the test setup shown in Figure 11.

A computer program was written for the IBM 1620 computer to solve Equation (12). Standard Fortran language was used and the FOR-TO-GO processor employed.

The base impedances of the active elements were estimated from graphs on monopole impedances in Schelkunoff and Friis (1952). The values were

$$Z_N = 37.5 + j21.5\ \Omega$$

$$Z_{N-1} = 25 - j22.5\ \Omega$$

$$Z_{N+1} = 70 + j75\ \Omega$$

$$Z_{N-2} = 16.5 - j40\ \Omega$$

The phase angles of the voltages "feeding" the elements in the active region were determined on the basis that the transmission line wave propagated at free-space velocity through the active region.

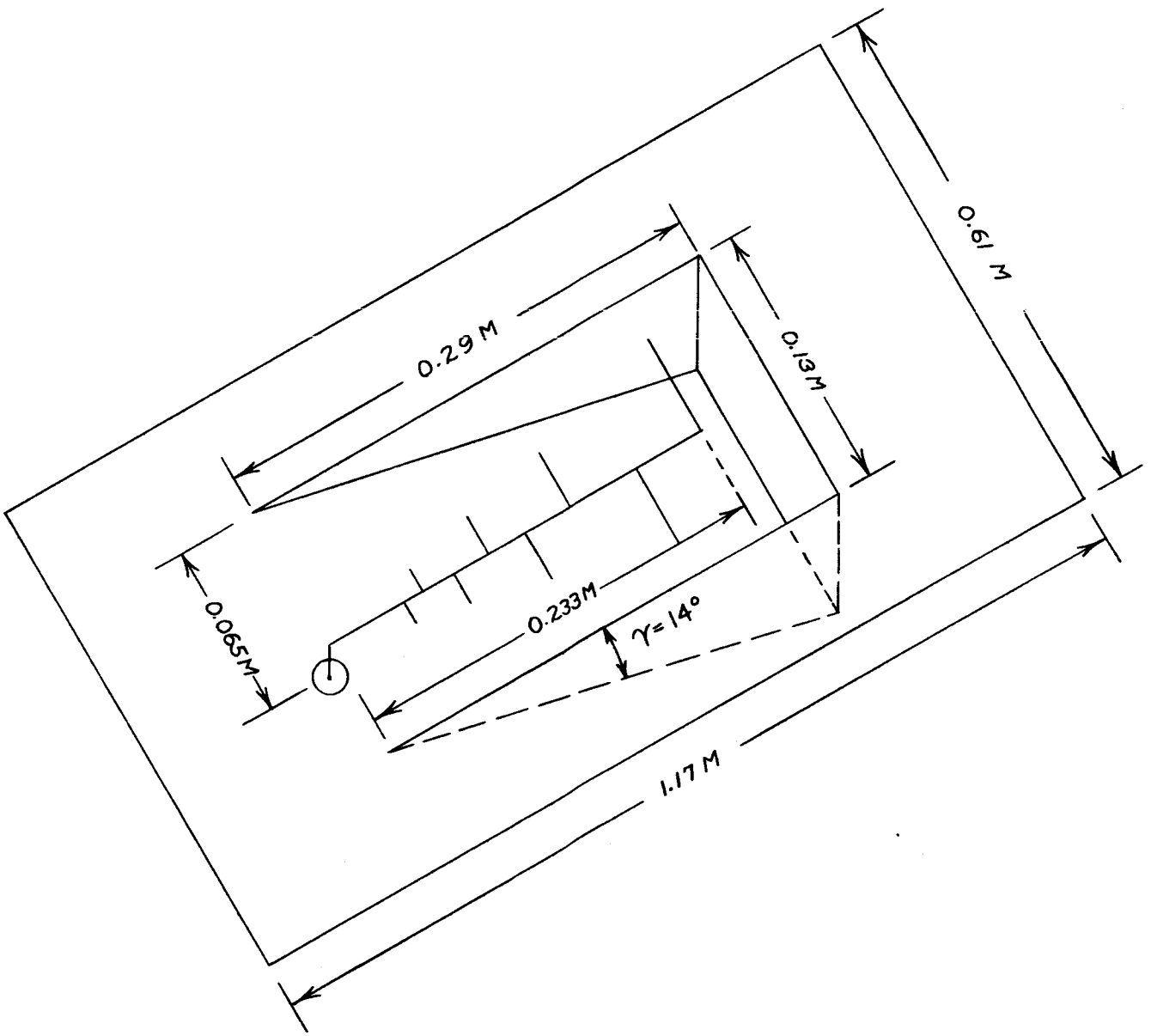

Figure 9. Perspective view of air-filled cavity.

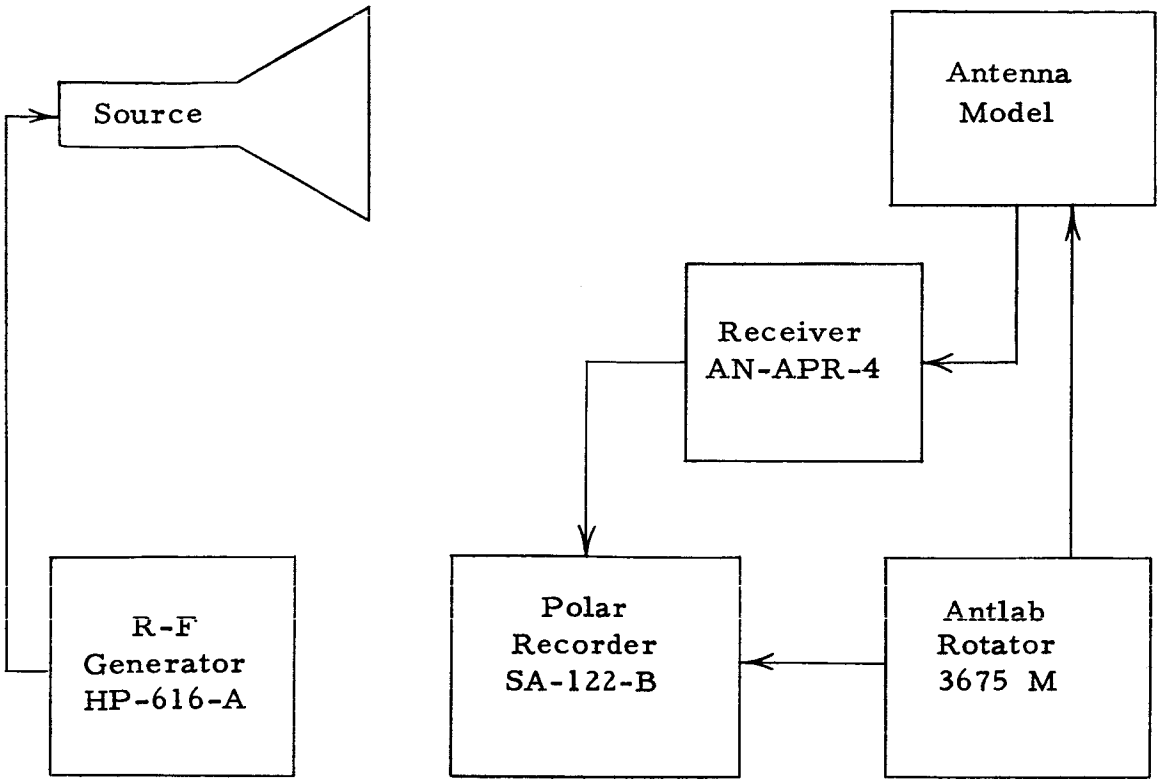

Figure 10. Pattern measurement arrangement.

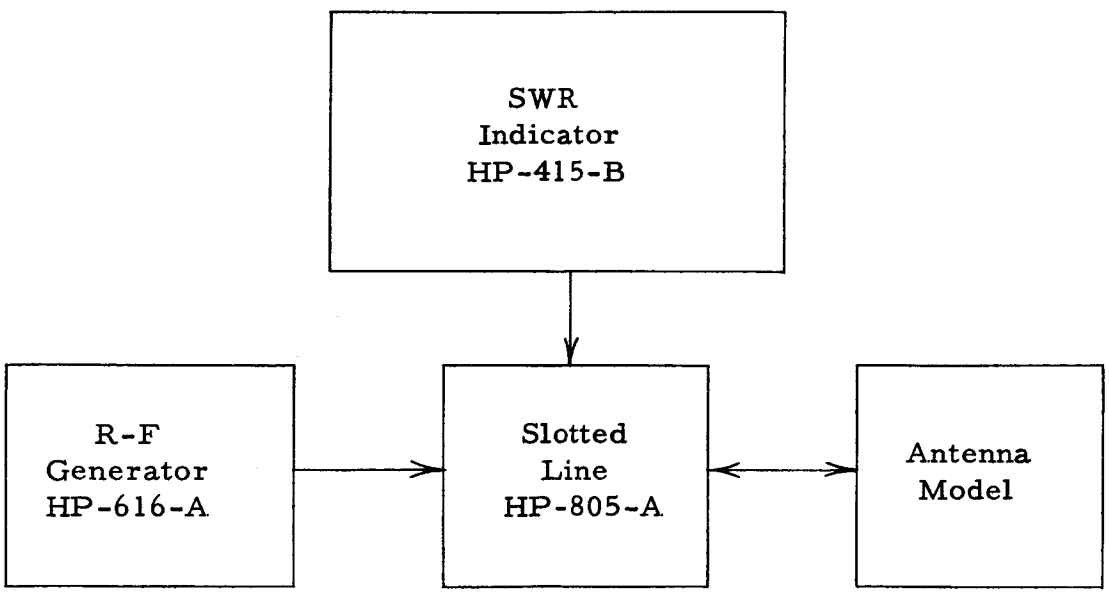

Figure 11. Impedance measurement arrangement.

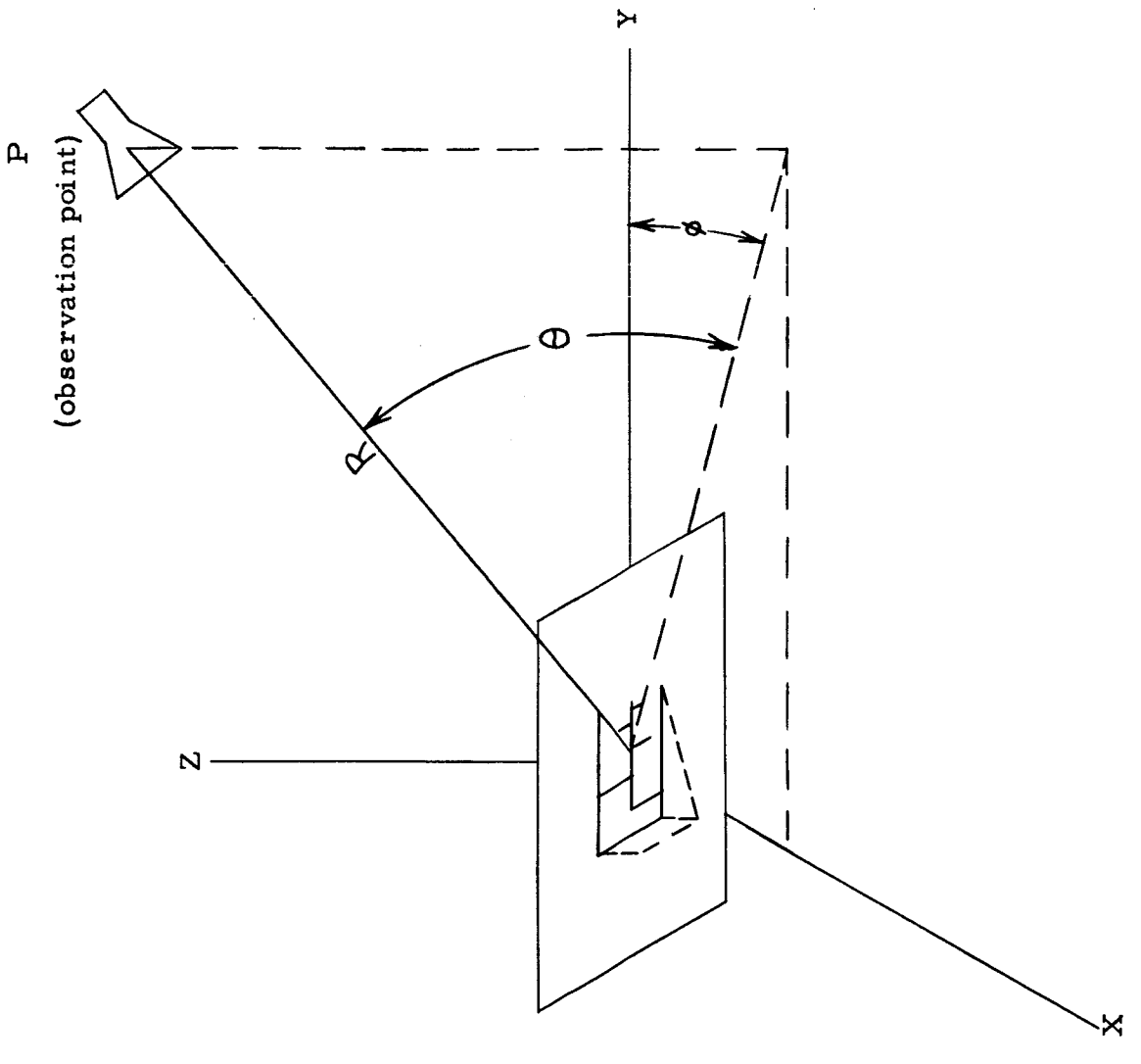

Figure 12. Coordinate system used for radiation field measurements.

The feeding phase angles are:

$$\delta_{N+1} = -1.12 \text{ radians}$$

$$\delta_{N-1} = 0.94 \text{ radians}$$

$$\delta_{N-2} = 1.77 \text{ radians}$$

The exponentials were calculated using the relationship

$$e^{jy} = 1 \angle y \tag{13}$$

Because the FOR-TO-GO processor is not capable of finding arccosines (only arctangents) the following relationship must be used:

$$\cos^{-1} y = \tan^{-1} \frac{\sqrt{1 - y^2}}{y} \tag{14}$$

However, the arctangent subroutine did not place the answer in the proper quadrant (it calculated only the principal value of the argument). Therefore, "if" statements were used to compare the algebraic signs of the numerator and denominator and place the answer in the proper quadrant accordingly.

The program was written such that one of the antenna design parameters could be varied while the others were held fixed. This procedure was used in gathering information for optimum antenna design.

Results

Figure 13 shows a comparison between the calculated and measured H-plane radiation patterns for the air-cavity mounted antenna.

Figure 14 is a plot of normalized measured impedance vs frequency for the antenna. Typical measured radiation patterns are presented in Figures 15 and 16, for $\tau = 0.85$, $a = 14^{o}$, and $\gamma = 14^{o}$.

Figures 17 and 18 are calculated H-plane pattern plots for various values of τ and γ.

Figures 19 and 20 present calculated information on how the half-power angle (δ) and the angle to the maximum point of radiation (θ_{max}) vary with τ and γ.

Tables 1 and 2 present specific information on the calculated H-plane radiation patterns while τ and γ are varied.

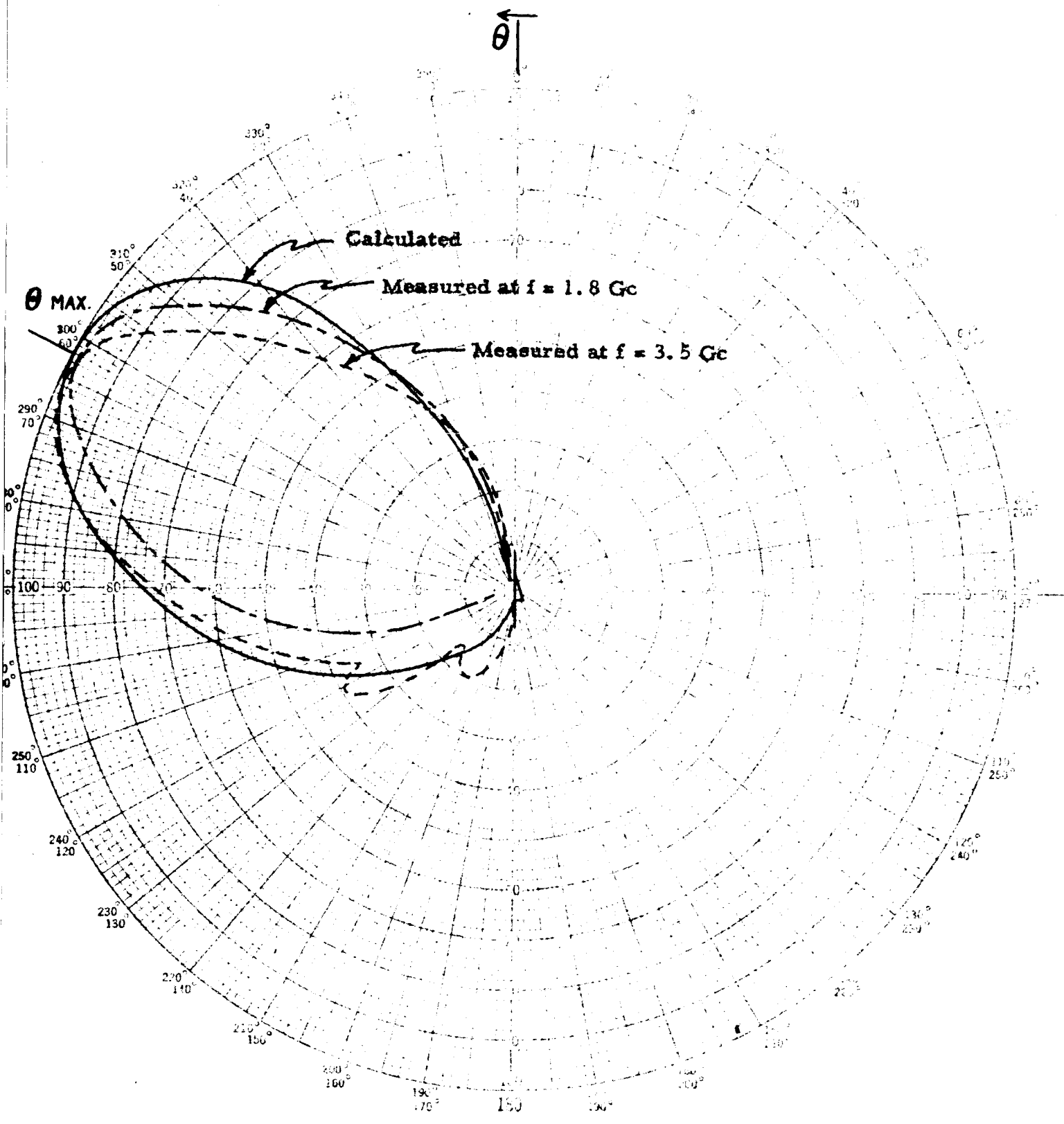

Figure 13. Linear voltage plots showing the comparison of measured and computed H-plane patterns, with $\tau = 0.85$, $\alpha = 14^{\circ}$, and $\gamma = 14^{\circ}$.

Polar Chart No. 127L

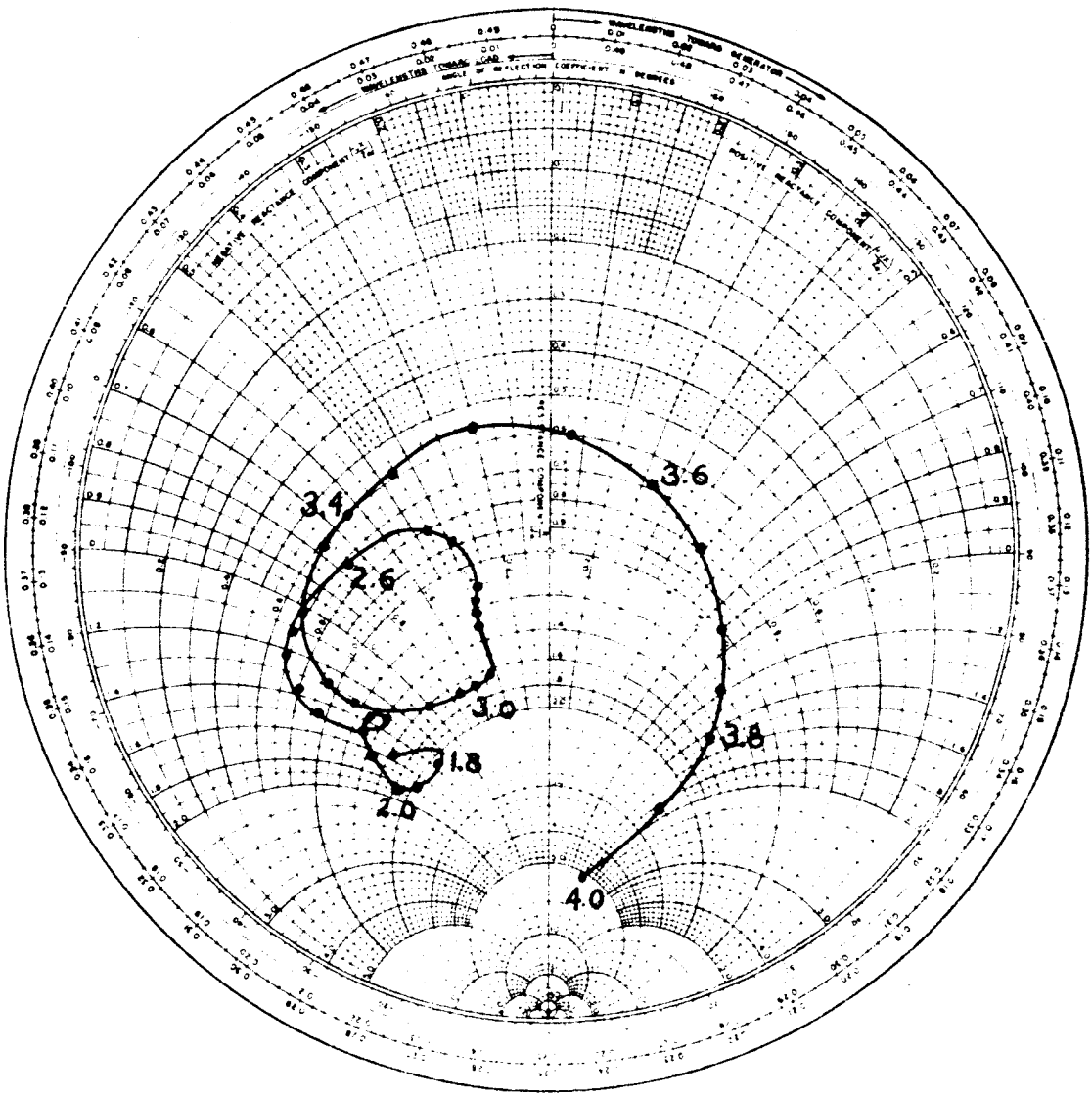

Figure 14. Measured antenna impedance normalized to 50 ohms. Frequencies are shown in Gc. The antenna is mounted over an air-filled cavity with $\tau = 0.85$, $\alpha = 14^{o}$, and $\gamma = 14^{o}$.

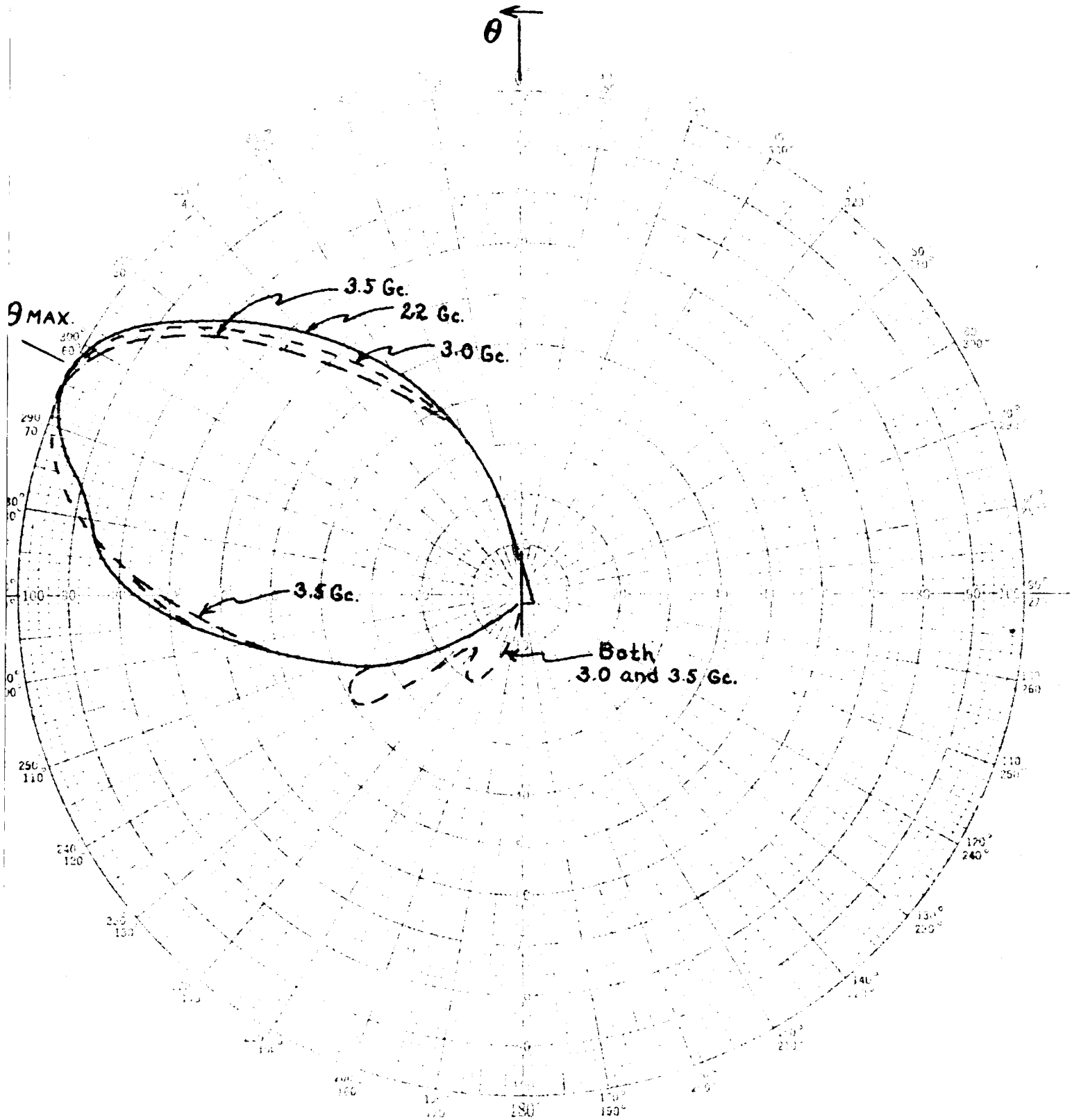

Figure 15. Measured H-plane pattern vs frequency. A linear voltage plot with $\phi = 0^{o}$ and θ = variable. The antenna is mounted over an air-filled cavity with $\tau = 0.85$, $a = 14^{o}$, and $\gamma = 14^{o}$.

Polar Chart No. 1

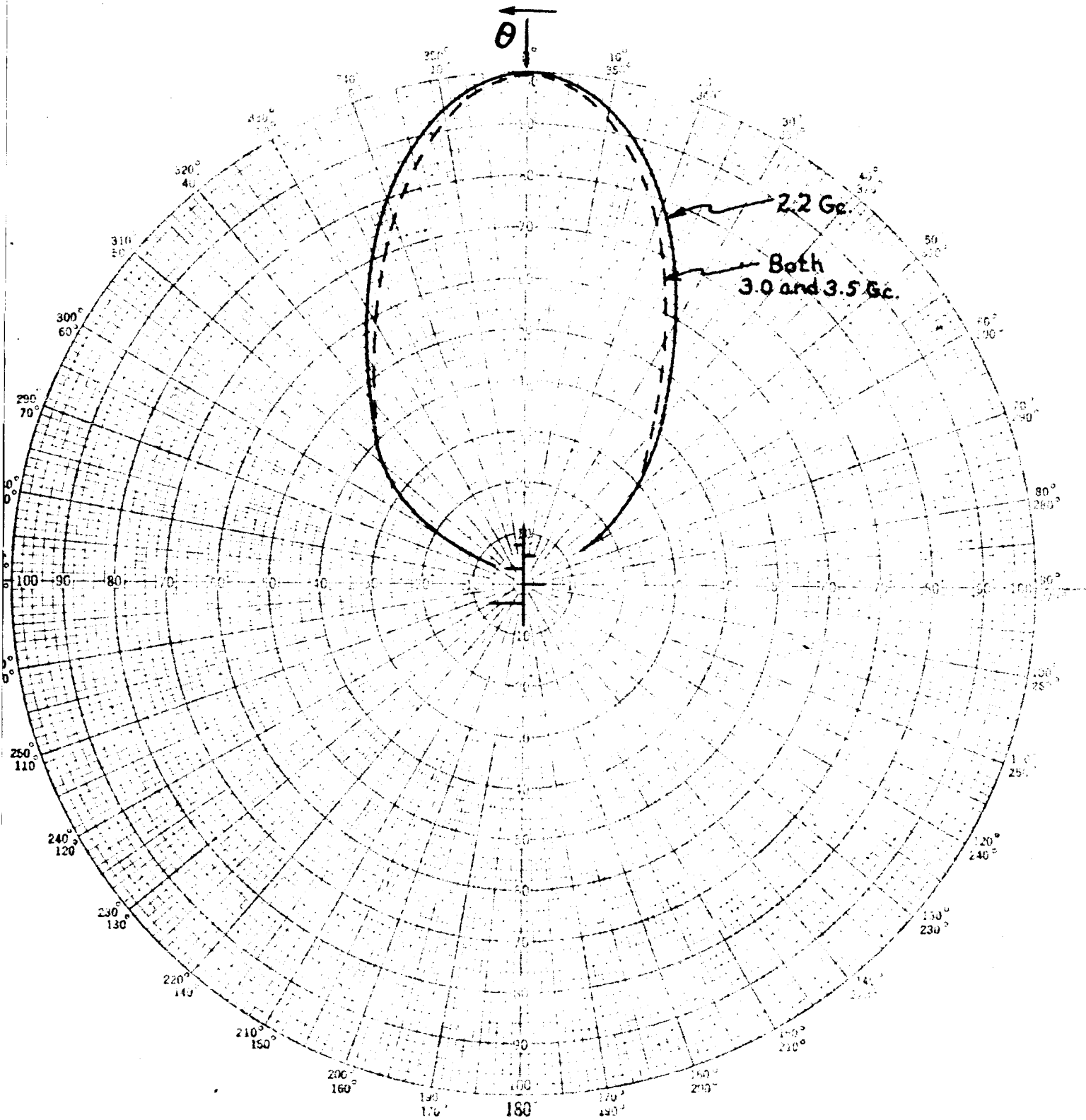

Figure 16. Measured E-plane pattern vs frequency. A linear voltage plot with $\phi = 0^{\circ}$ and θ = variable. The antenna is mounted over an air-filled cavity with $\tau = 0.85$, $\alpha = 14^{\circ}$, and $\gamma = 14^{\circ}$.

Polar Chart No. 127L

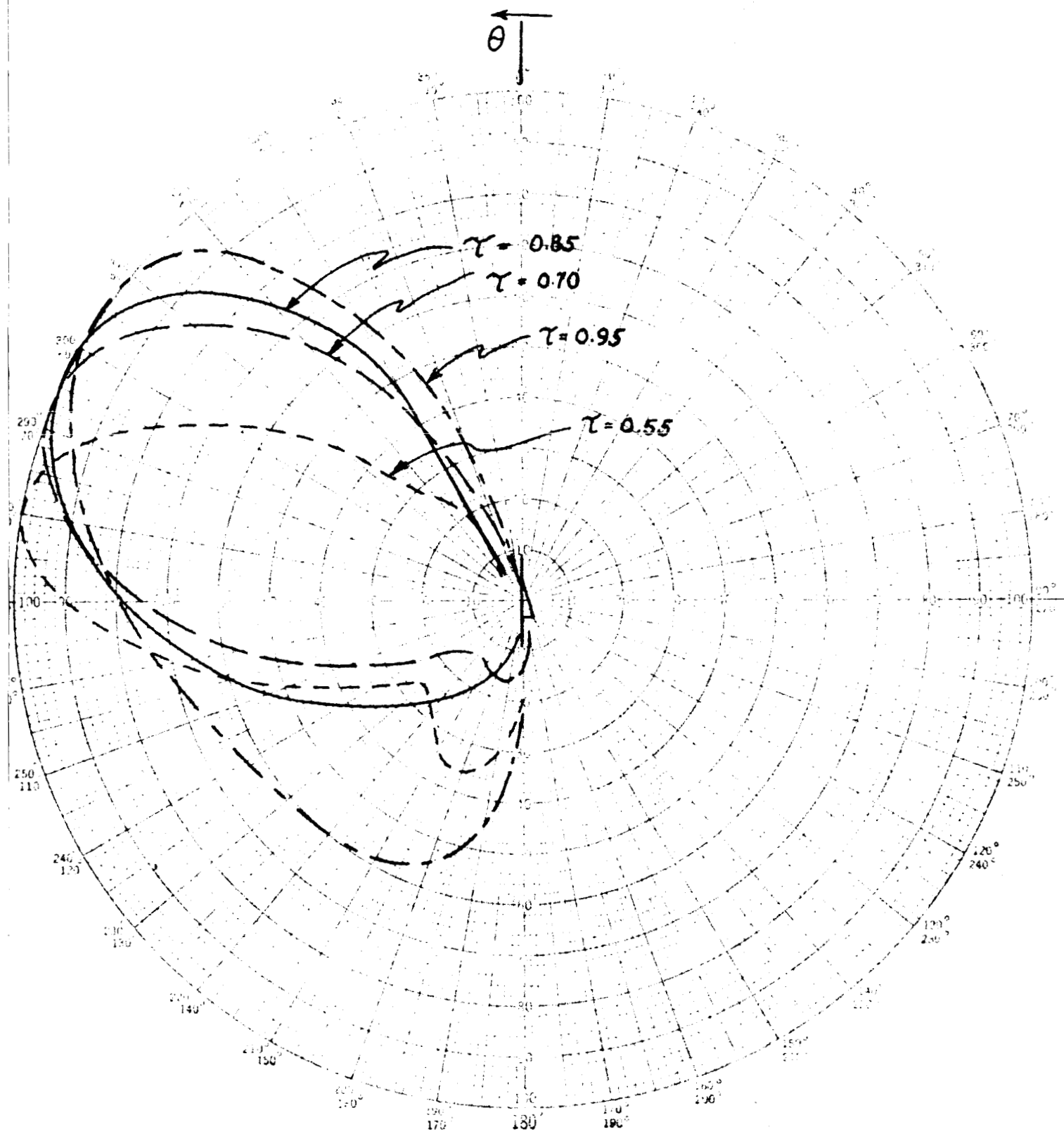

Figure 17. Calculated H-plane radiation pattern vs τ for $\gamma = 14^{o}$. (A linear voltage plot.) γ is the cavity floor angle.

Polar Chart No. 1272

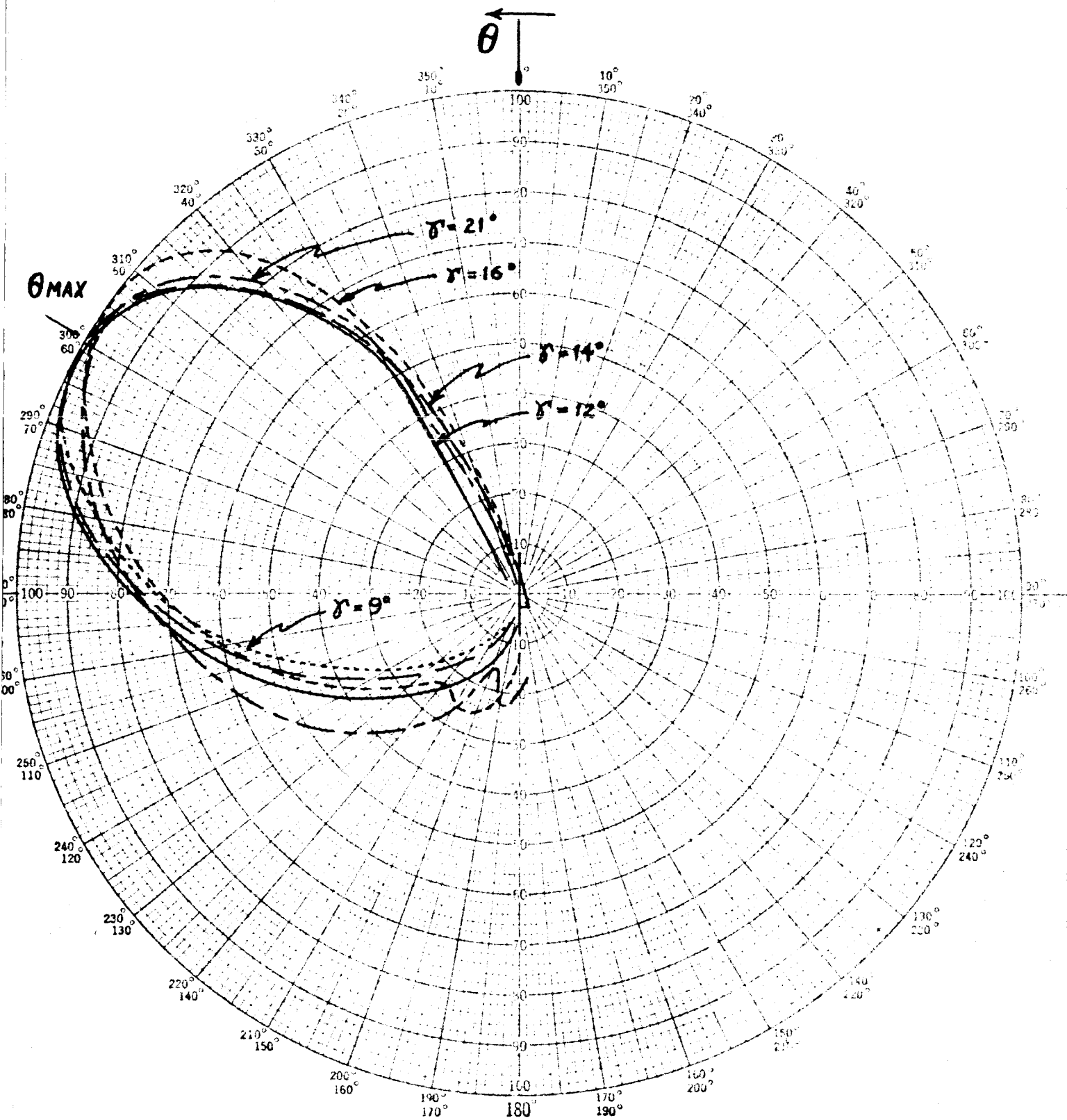

Figure 18. Calculated H-plane radiation pattern vs γ for $\tau = 0.85$. (A linear voltage plot.) γ is the cavity-floor angle.

Polar Chart No. 127L

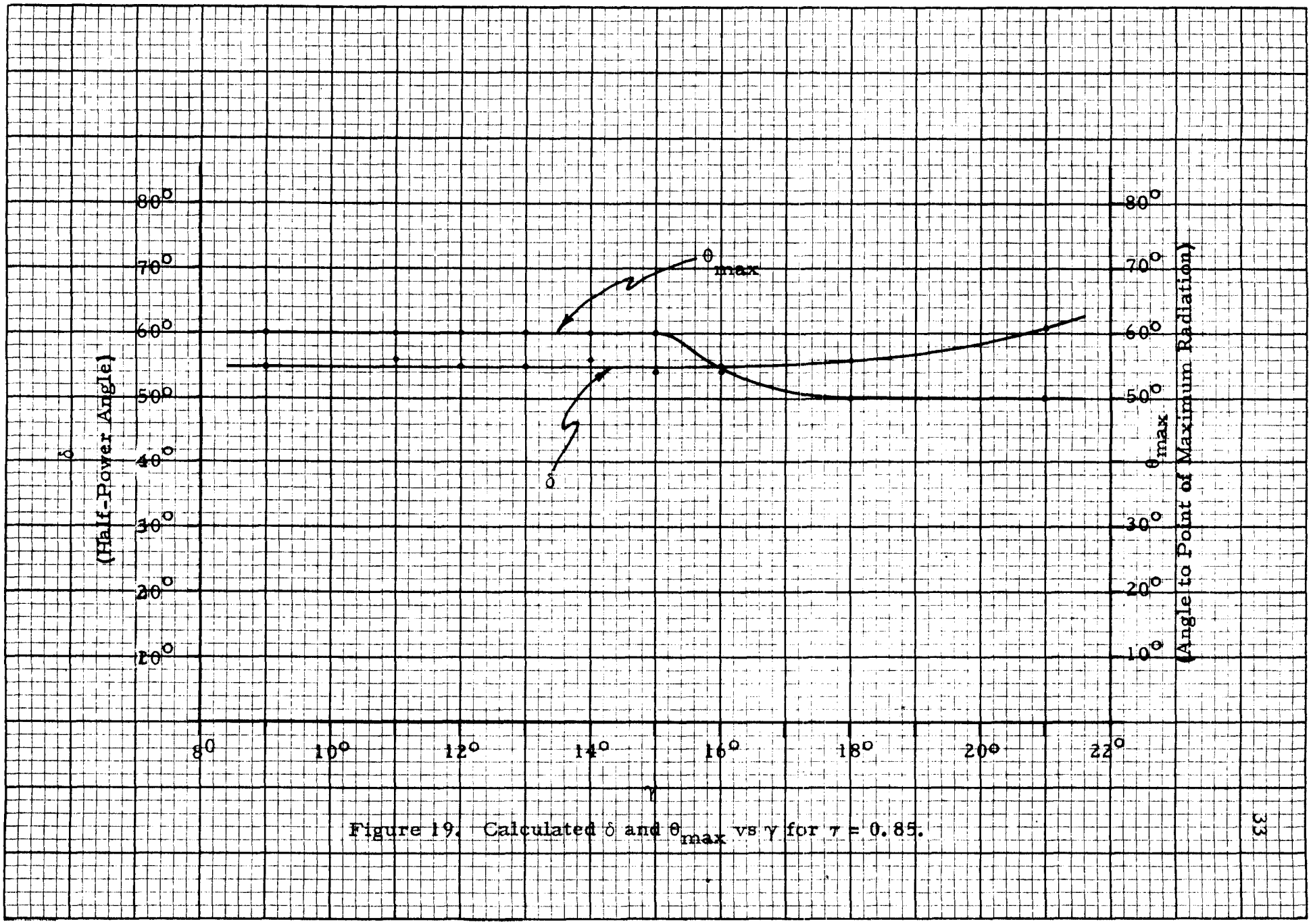

Figure 19. Calculated δ and θ_{max} vs γ for $\tau = 0.85$.

Table 1. H-plane radiation data for calculated patterns with $\tau = 0.85$, γ = variable.

γ	τ	Half-Power Angle	Angle of Peak Radiation	Comments
9^{o}	0.85	55^{o}	60^{o}	
11^{o}	0.85	56^{o}	60^{o}	
12^{o}	0.85	55^{o}	60^{o}	
13^{o}	0.85	55^{o}	60^{o}	
14^{o}	0.85	56^{o}	60^{o}	
15^{o}	0.85	54^{o}	60^{o}	
16^{o}	0.85	54^{o}	55^{o}	Side Lobe at 160^{o}
18^{o}	0.85	56^{o}	50^{o}	Side Lobe at 163^{o}
21^{o}	0.85	61^{o}	50^{o}	Side Lobe at 170^{o}

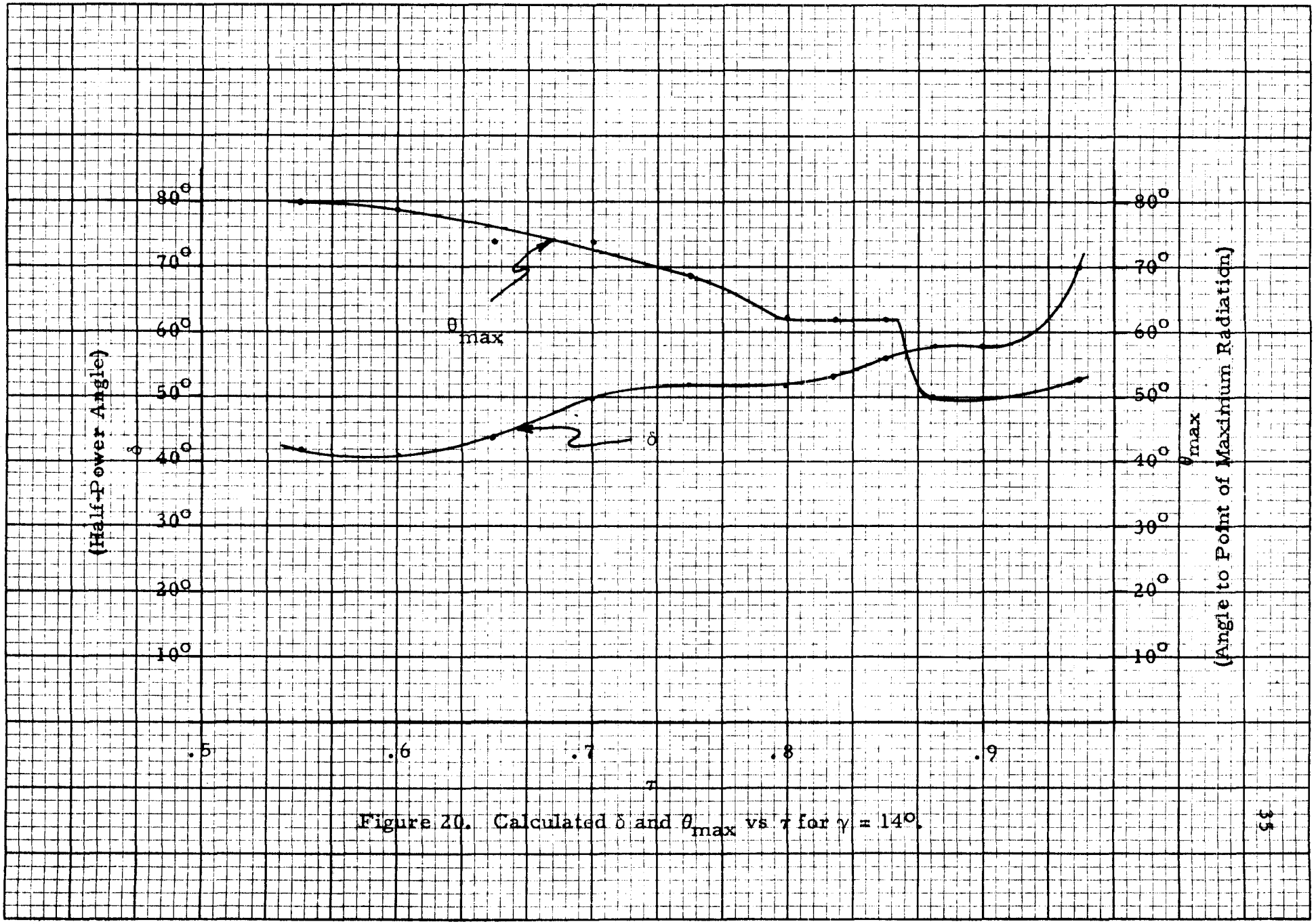

Figure 20. Calculated δ and θ_{max} vs τ for γ = 14°.

Table 2. H-plane radiation data for calculated patterns with $\gamma = 14^{\circ}$, τ = variable.

γ	τ	Half-Power Angle	Angle of Peak Radiation	Comments
14°	.55	42°	80°	Pattern is much narrower, large side lobe at 160°
14°	.6	41°	75°	Pattern has narrowed up, large side lobe at 160°
14°	.65	44°	70°	Small side lobe at 160°
14°	.7	50°	70°	Small side lobe at 170°
14°	.75	52°	65°	Small side lobe developing at 170°
14°	.8	52°	60°	
14°	.83	53°	60°	
14°	.85	56°	60°	
14°	.88	58°	50°	Large side lobe developing at 160°
14°	.9	58°	50°	Large side lobe at 160° Pattern is more broad over last half
14°	.95	69°	53°	Pattern very much widened

DISCUSSION AND CONCLUSIONS

In a previous section the basic normalized H-plane radiation pattern equation, Equation (12), was derived for an air-filled cavity. A program was written for the IBM 1620 computer to solve this equation for various values of θ. Figure 13 shows the close agreement between the calculated pattern and the measured patterns with $\tau = 0.85$, $\alpha = 14^{\circ}$ and $\gamma = 14^{\circ}$. This close agreement illustrates that the assumptions and approximations made in deriving this equation are reasonably correct. These assumptions were:

(1) The energy from the antenna is radiated from an active-element array (in our case 4 elements) which changes position as the excitation frequency is varied;

(2) The currents alternate down the active-element array;

(3) The active region can be determined by estimating the base impedance of each element at the operating frequency;

(4) The center rod of the antenna acts as a transmission line;

(5) The voltage wave, feeding the active region, remains approximately constant in magnitude but varies in phase over this region.

Figure 14 illustrates that the test antenna design is log-periodic. Its impedance essentially repeats periodically with the logarithm of the frequency. The general impedance spiral is in the area of low VSWR.

Figures 15 and 16 show that the shapes and the directions of the antenna's measured patterns vary slightly with frequency over the designed frequency band.

The following conclusions are based on computed data. Figures 17 and 20 illustrate how the H-plane radiation patterns vary with τ for $\gamma = 14^{\circ}$. It is interesting to note that as τ increases, θ_{max} (the angle to the point of maximum radiation) decreases while δ (the half-power angle) increases. The point of intersection of the curves on Figure 20 occurs at $\tau = 0.86$, very nearly equal to the value of $\tau = 0.85$ used in the actual constructed model. At low and at high values of τ the pattern changes considerably indicating that these extremes should be avoided in actual antenna design or that perhaps the assumptions made in deriving the H-plane pattern equation are not correct at these extremes. In any case, to avoid the formation of side lobes (see Table 2) τ should be held within the range $.75 \leq \tau \leq .85$ (for $\gamma = 14^{\circ}$).

Figures 18 and 19 illustrate how the H-plane radiation patterns vary with γ (the cavity-floor angle) for $\tau = 0.85$. Both the half-power angle (δ) and the angle to the maximum point of radiation (θ_{max}) are constant over the range $9^{\circ} \leq \gamma \leq 15^{\circ}$, but deviate from these constant values when γ exceeds 15°. Table 1 indicates that side lobes do not form until γ exceeds 15°. Thus it would seem that any γ in the range $9^{\circ} \leq \gamma \leq 15^{\circ}$ would be satisfactory for the antenna design. However, the effect on impedance must be considered. Clark, Jones, and Leigh

(1960) experimentally investigated the effect of γ variations on the average deviations of the impedance from a reference value as frequency is changed and found that the average deviation is minimum for $\gamma = 15^{o}$. This would suggest that the optimum value of γ is 15^{o}. Fifteen degrees is the optimum value for γ, because at 15^{o} the distance from the resonant element to its image is $\lambda_N/2$.

To summarize: It seems clear that 15^{o} is the optimum angle for γ while the optimum value of τ lies in the range $.75 \leq \tau \leq .85$.

SUGGESTIONS FOR FUTURE WORK

The following areas of study are suggested for future work.

(1) Determine the effect that τ has on the driving point impedance to further optimize the value of τ.

(2) Determine the true values of the driving-point impedance at various frequencies.

(3) Measure the current distribution (magnitude and phase) and the wave velocity on the antenna elements in the active region.

(4) Study the antenna design for operation over a 10:1 frequency range.

(5) Study impedance characteristics with a wide-band transformer to convert the natural antenna impedance to that of the measuring equipment.

LITERATURE CITED

Bell, R. L., C. T. Elfving and R. E. Franks, 1960, "Near-Field Measurements on a Logarithmically Periodic Antenna," IRE Transactions, Vol. AP-8, pp. 559-567; November.

Brownell, Fred P., 1961, "Radiation and Impedance Characteristics of a Log-Periodic Antenna Structure Near a Conducting Surface," Unpublished M. S. Thesis, Utah State University Library, Logan, Utah.

Clark, C., W. L. Jones, and A. Leigh, 1962, "A Theoretical and Experimental Investigation of Flush Mounting Configurations for Log-Periodic Structures," Utah State University Engineering Experiment Station Report.

DuHamel, R. H., and D. E. Isbell, 1957, "Broadband Logarithmically Periodic Antenna Structures," IRE National Convention Record, Vol. 5, Pt. 1, pp. 119-128.

DuHamel, R. H., and F. R. Ore, 1958, "Logarithmically Periodic Antenna Designs," IRE National Convention Record, Vol. 6, Pt. 1, pp. 139-151.

Isbell, D. E., 1960, "Log Periodic Dipole Arrays," IRE Transactions, Vol. AP-8, pp. 260-267; May.

Schelkunoff, S. A., and H. T. Friis, 1952, Antennas: Theory and Practice, John Wiley and Sons, Inc., New York.

Whale, R. L., and C. Clark, 1963, "A Log Periodic Monopole Antenna in a Dielectric-Filled Cavity," Utah State University Engineering Experiment Station Report; June 30.

N64-29703

APPENDIX B

THE RADIATION PATTERNS OF A LOG PERIODIC MONOPOLE ANTENNA

by

Ming-hui Chen

ACKNOWLEDGEMENTS

The assistance of Dr. Clayton Clark, Dr. Craig Rushforth and Mr. G. Paul Francis of the Electrical Engineering Department of Utah State University is gratefully acknowledged.

This work was supported by the National Aeronautics and Space Administration under Grant NsG-221-62.

Ming-hui Chen

TABLE OF CONTENTS

LIST OF FIGURES

INTRODUCTION

The log periodic monopole antenna is one type of frequency independent antenna. It consists of a number of monopole elements mounted upon a center feed line. The length of the monopole elements and the distance between each element and the feed point are both increasing in logarithmic ratio [1].

This antenna has one resonant element and many (usually 4 to 7) nonresonant elements for each frequency. New elements at a different position on the center feed line become resonant when the frequency changes. The new resonant element and its associated elements appear exactly as the previous set at the original frequency Therefore, the radiation patterns of this atenna are independent of frequency.

ABST

2 9703

In this thesis, two general equations of radiation patterns are derived. One is a three-dimensional radiation pattern in air. The other is a two-dimensional radiation pattern (H-plane) when the source is immersed in a dielectric medium. The patterns were calculated on the USU IBM 1620 computer and compared with the measured patterns.

Author

In the derivation of these radiation patterns the following assumptions have been made:

(1) The connecting points of each element and the center feed line have the same potential.

(2) The mutual impedance between elements make a negligible contribution to the element impedance.

(3) Reflecting surfaces are assumed perfect.

(4) Cavity side wall and end watt effects are assumed negligible.

THE RADIATION PATTERNS OF A LOG PERIODIC MONOPOLE ANTENNA WITH A REFLECTING PLANE

The structure of the log periodic antenna is shown in Figure 1. The length of the nth element is $L_{n\ell}$ and the distance from the feed point to the nth element is S_n.

The taper angle a is defined as

$$a = \tan^{-1} \frac{L_n}{S_n} \tag{1}$$

The logarithmic ratio parameter τ is defined as

$$\tau = \frac{L_{n-1}}{L_n} = \frac{S_{n-1}}{S_n} \tag{2}$$

The angle between the antenna and the reflecting plane is γ. The antenna coordinate system is shown in Figure 2.

Each element has a self impedance which is dependent upon the length L_k. It can be expressed as

$$\overset{s}{Z}_k = Z_k \underline{/\theta_k} \tag{3}$$

The current on the terminal of the Kth element is

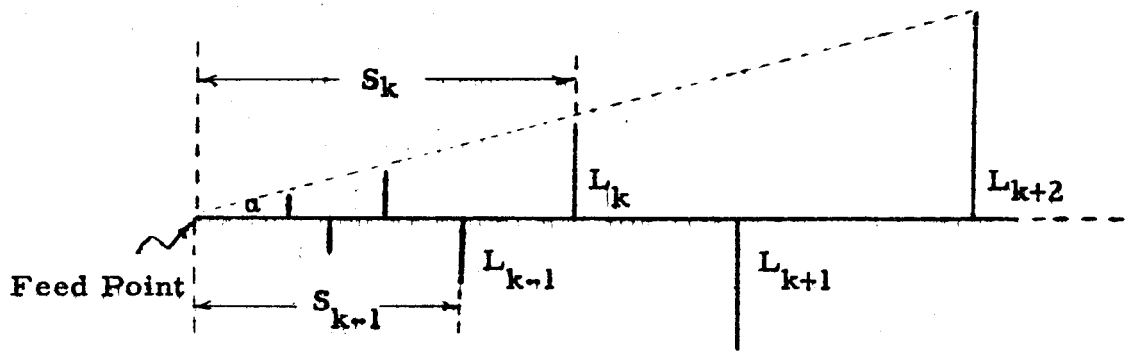

Figure 1, The structure of the log periodic monopole antenna.

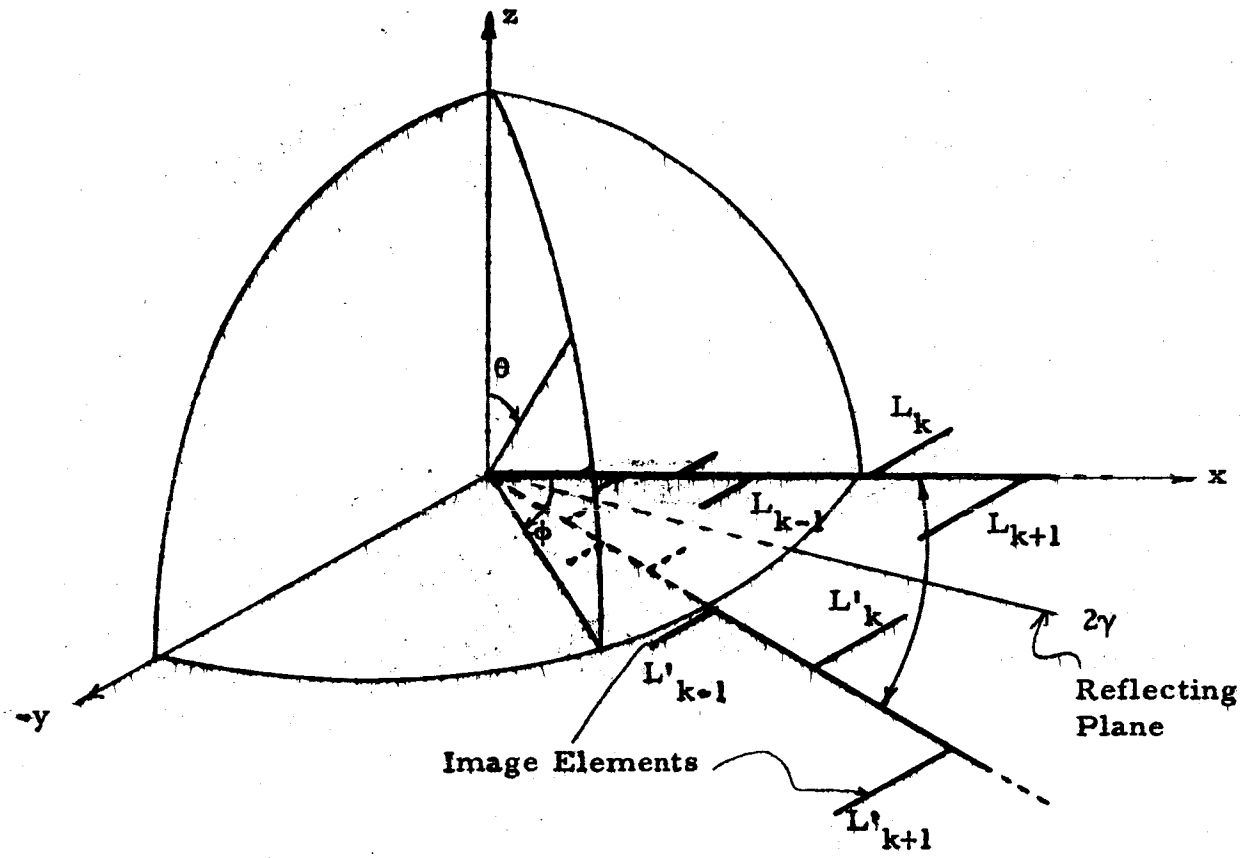

Figure 2. The coordinate system.

$$\dot{I}_k(0) = \frac{V}{Z_k} \angle -\beta S_k - \theta_k \qquad (4)$$

The current distribution on the Kth element is assumed to be sinusoidal such as

$$I_k(y) = (I_k)_m \sin \beta(L_k - |y|) \qquad (5)$$

The radiation function of this type antenna is found to be (see Appendix)

$$F_\theta(\theta,\phi,\alpha,\gamma,\tau) = \frac{\cos\theta\sin\phi}{1-\sin^2\theta\sin^2\phi}\left\{\sum_{k=0}^{\infty}\frac{e^{-j\left(\frac{\pi}{2}\tau^{n-k}\cot\alpha+\theta_k\right)}}{Z_k\sin\left(\frac{\pi}{2}\tau^{n-k}\right)}\cdot\right.$$

$$\left[e^{j\frac{\pi}{2}\tau^{n-k}\cot\alpha\sin\theta\cos\phi} - e^{j\frac{\pi}{2}\tau^{n-k}(\cos2\gamma\sin\theta\cos\phi-\sin2\gamma\cos\theta)\cot\alpha}\right]\cdot \qquad (6)$$

$$\left.\left[(-1)^{n-k}e^{j(-\tau)^{n-k}\frac{\pi}{2}\sin\theta\sin\phi} - (-1)^{n-k}\cos\left(\frac{\pi}{2}\tau^{n-k}\right) - j\sin\theta\sin\phi\sin\left(\frac{\pi}{2}\tau^{n-k}\right)\right]\right\}$$

$$F_\phi(\theta,\phi,\alpha,\gamma,\tau) = \frac{\cos\phi}{1-\sin^2\theta\sin^2\phi}\left\{\sum_{k=0}^{\infty}\frac{e^{-j\left(\frac{\pi}{2}\tau^{n-k}\cot\alpha+\theta_k\right)}}{Z_k\sin\left(\frac{\pi}{2}\tau^{n-k}\right)}\cdot\right.$$

$$\left[e^{j\frac{\pi}{2}\tau^{n-k}\cot\alpha\sin\theta\cos\phi} - e^{j\frac{\pi}{2}\tau^{n-k}(\cos2\gamma\sin\theta\cos\phi-\sin2\gamma\cos\theta)\cot\alpha}\right]\cdot \qquad (7)$$

$$\left.\left[(-1)^{n-k}e^{j(-\tau)^{n-k}\frac{\pi}{2}\sin\theta\sin\phi} - (-1)^{n-k}\cos\left(\frac{\pi}{2}\tau^{n-k}\right) - j\sin\theta\sin\phi\sin\left(\frac{\pi}{2}\tau^{n-k}\right)\right]\right\}$$

and

$$E_\theta(\theta,\ \phi,\ \alpha,\ \gamma,\ \tau) = \frac{j\omega\mu V e^{-j\beta r_o}}{4\pi r_o\beta}\ F_\theta(\theta,\ \phi,\ \alpha,\ \gamma,\ \tau) \qquad (8)$$

$$E_\phi(\theta,\ \phi,\ \alpha,\ \gamma,\ \tau) = \frac{j\omega\mu V e^{-j\beta r_o}}{4\pi r_o\beta}\ F_\phi(\theta,\ \phi,\ \alpha,\ \gamma,\ \tau) \qquad (9)$$

The substitution of $\phi = 0^{\circ}$ into Equation (6) and Equation (7) leads to the function in the H-plane ($\phi=0^{\circ}$ plane)

$$F_{\theta} = (\theta,\ 0,\ \alpha,\ \gamma,\ \tau) = 0 \tag{10}$$

$$F_{\phi}(\theta, 0, \alpha, \gamma, \tau) = \sum_{k=0}^{\infty} \frac{e^{-j\left(\frac{\pi}{2}\tau^{n-k}\cot\alpha + \theta_k\right)}}{Z_k \sin\left(\frac{\pi}{2}\tau^{n-k}\right)} (-1)^{n-k} \cdot \left[1-\cos\left(\frac{\pi}{2}\tau^{n-k}\right)\right] \cdot \left[e^{j\frac{\pi}{2}\tau^{n-k}\cot\alpha\sin\theta} - e^{j\frac{\pi}{2}\tau^{n-k}\sin(\theta-2\gamma)\cot\alpha}\right] \tag{11}$$

The substitution of $\theta = 90^{\circ}$ into Equation (6) and Equation (7) leads to the function in the E-plane ($\theta=90^{\circ}$ plane)

$$F_{\theta}\ (90^{\circ},\ \phi,\ A,\ \gamma,\ \tau) = 0 \tag{12}$$

$$F_{\phi}(90^{\circ}, \phi, \alpha, \gamma, \tau) = \frac{1}{\cos\phi} \sum_{k=0}^{\infty} \left\{ \frac{e^{-j\left(\frac{\pi}{2}\tau^{n-k}\cot\alpha + \theta_k\right)}}{Z_k \sin\left(\frac{\pi}{2}\tau^{n-k}\right)} \cdot \left[e^{j\frac{\pi}{2}\tau^{n-k}\cot\alpha\cos\phi} - e^{j\frac{\pi}{2}\tau^{n-k}\cos2\gamma\cos\phi\cot\alpha}\right] \cdot \left[(-1)^{n-k} e^{j(-1)^{n-k}\frac{\pi}{2}\sin\phi} - (-1)^{n-k}\cos\left(\frac{\pi}{2}\tau^{n-k}\right) - j\sin\phi\sin\left(\frac{\pi}{2}\tau^{n-k}\right)\right]\right\} \tag{13}$$

The H-plane radiation pattern from Equation (11) and the experimental radiation pattern are plotted on Figure 3.

Figure 4 shows the construction of the air cavity used for this experiment. It was a little different with the conditions of theoretical derivation, so that the theoretical and experimental patterns on Figure 3 will not coincide except in the region of $-60^{\circ} < \theta < +30^{\circ}$.

As Figure 4 shows, power radiated by the image elements cannot be received in the region of $-90^{\circ} < \theta < -60^{\circ}$. Because of the vertical

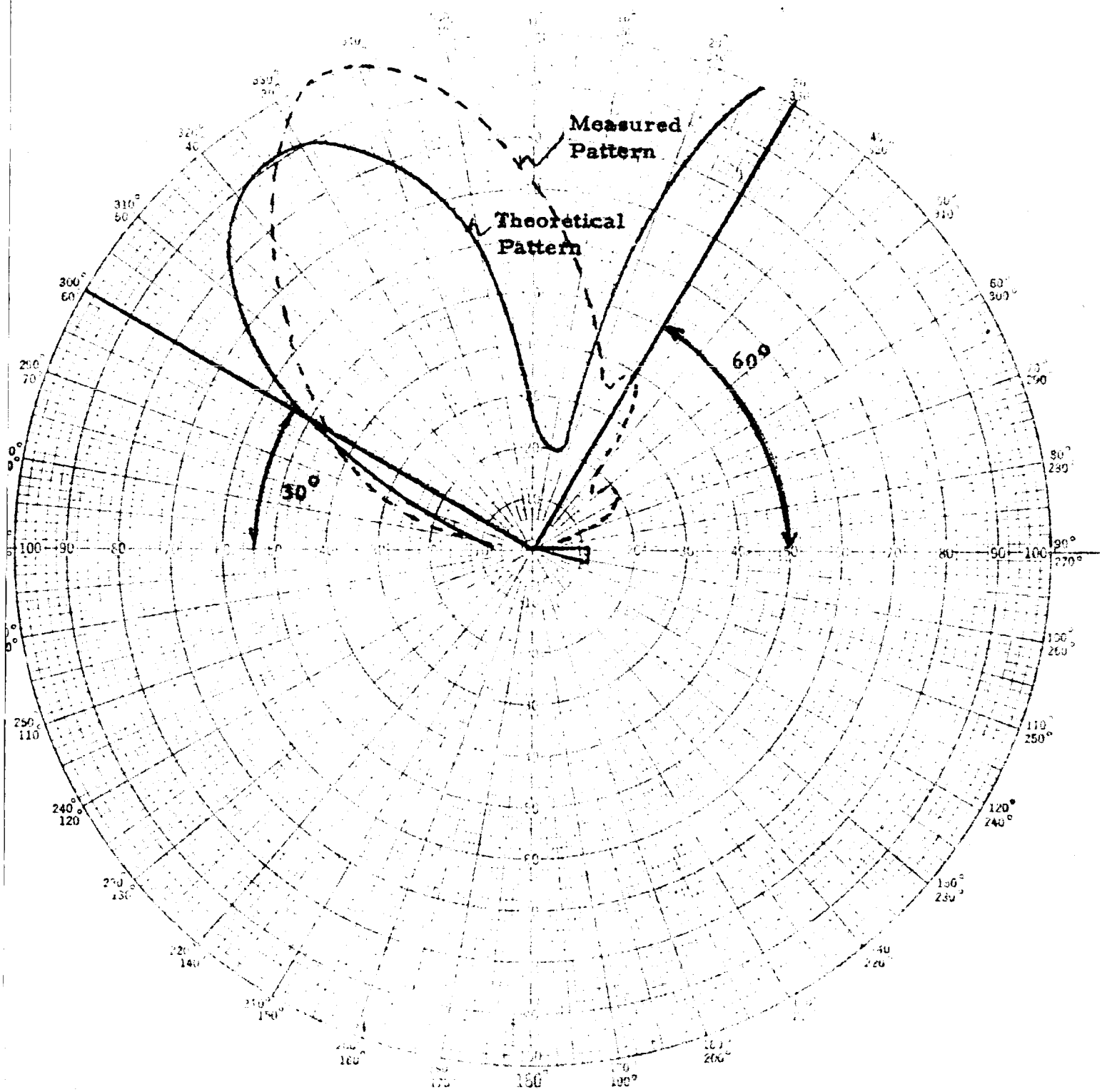

Figure 3. H-plane patterns, $\epsilon_r = 1.0$.
$\alpha=14^\circ$, $\tau=0.85$, $\gamma=15^\circ$, $\epsilon_r=1.0$, $\phi=0^\circ$

Polar Chart No. 127

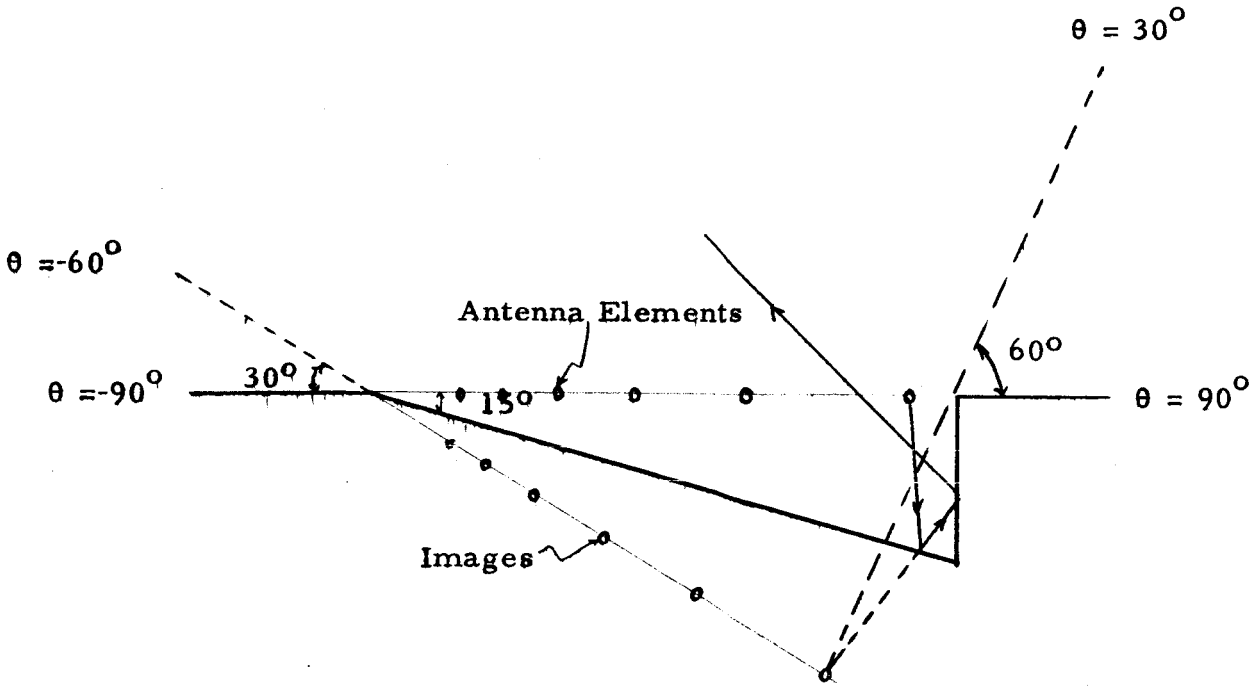

Figure 4, The construction of the air cavity.

plane of the cavity, the image of last element cannot radiate power to the region of $30^{\circ} < \theta < 90^{\circ}$, so that it is meaningless to discuss this region. The theoretical pattern of Figure 3 shows that the radiated power in $30^{\circ} < \theta < 0^{\circ}$ region is larger than the main lobe in $-60^{\circ} < \theta < 0^{\circ}$ region. This does not agree with the experimental results, but we know that the backward power was reflected to the forward direction by the vertical plane of the cavity, as the ray diagram shows in Figure 4. Therefore, the forward power becomes larger. We believe that this is the reason why the experimental results have a larger lobe at the forward than in the backward direction.

The equation of the plane which makes an angle γ with the $\theta = 90^{\circ}$ plane is

$$\cos \phi = \cot \gamma \cot \theta \tag{14}$$

The solution of Equation (14) and Equation (6) is the θ direction field on the plane described by Equation (14). The solution of Equation (14) and Equation (7) is the ϕ direction field on the same plane. Figure 3 shows that the maximum power direction is at $\gamma = 120^{\circ}$. Therefore, we plot the plane radiation pattern on Figure 5 at $\gamma = 120^{\circ}$.

Figure 5 shows that the theoretical pattern shows a wider beam width than the experimental pattern. This is probably due to the physical construction of the cavity. The two vertical planes on the

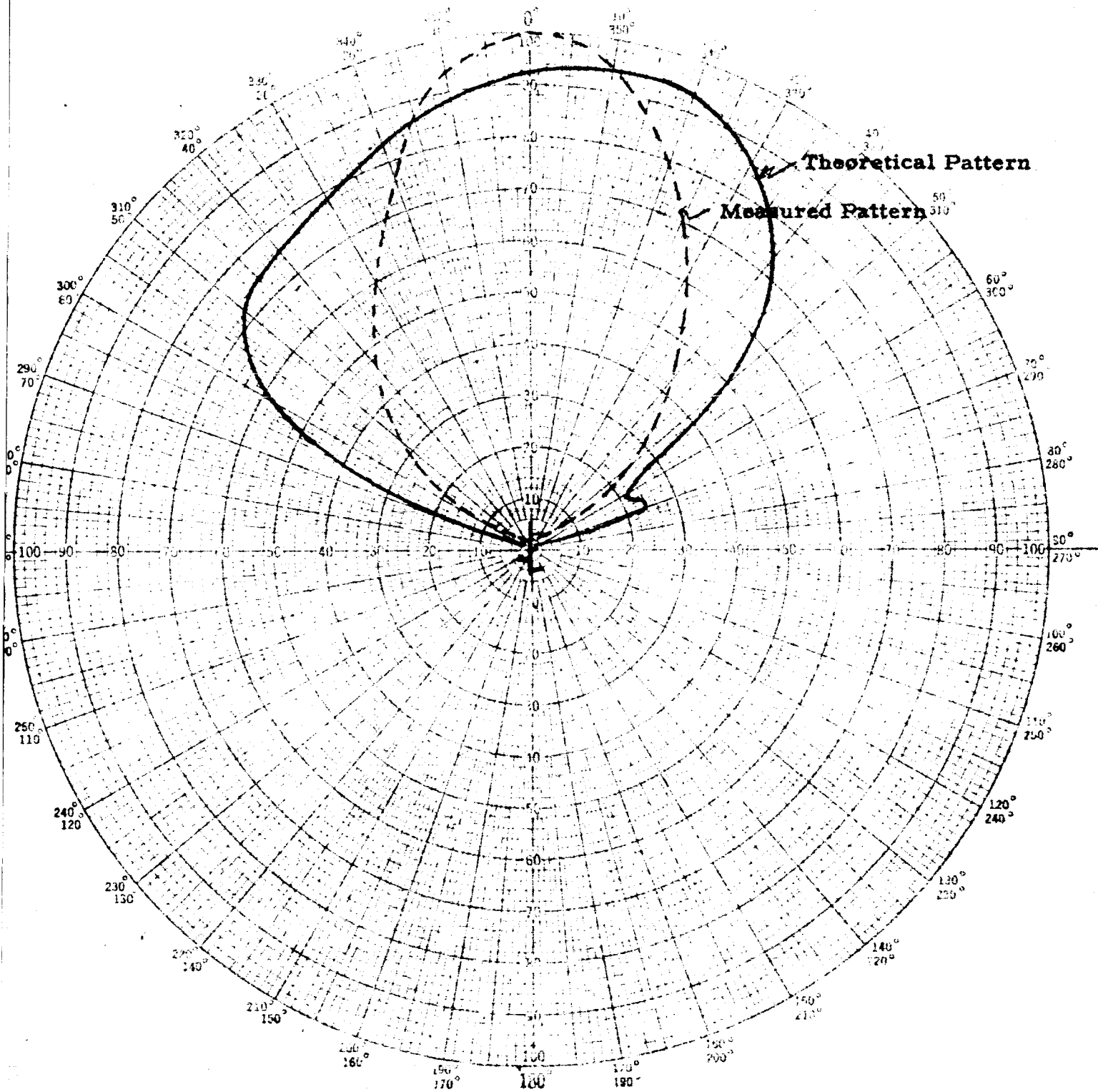

Figure 5. E-plane patterns, $\epsilon_r = 1.0$.

$\alpha = 14^\circ$, $\gamma = 15^\circ$, $\tau = 0.85$, $\beta = 120^\circ$

Polar Chart No. 12/L

side of the cavity prevent the images of elements from radiating power in the full E-plane. It appears that reflections from the sides contribute to the energy radiated near the center part of the E-plane pattern. The result is a narrower experimental E-plane pattern than the calculated pattern.

THE RADIATION PATTERN OF A LOG PERIODIC MONOPOLE ANTENNA IN A DIELECTRIC MEDIUM

The antenna described previously was placed in a dielectric medium for the purpose of reducing the required cavity volume and to increase mechanical rigidity. The section describes results of calculations made with the IBM 1620 computer to determine the theoretical patterns of the dielectric covered models. Figure 6 shows this arrangement.

Due to the influence of the dielectric surface and the conducting plane, power cannot radiate directly. Part of it radiates after one refraction; part of it after several reflections and one refraction. These rays can be divided into two groups: One contains the rays after an even number of reflections and one refraction (i. e., the rays arrive at the dielectric surface first), the other contains the rays after an odd number of reflections and one refraction (i. e., the rays arrive at the conducting plane first).

The power radiated by the ray after a different number of reflections can be thought of as if it were radiated by the different images. Therefore, we can divide the images in two groups: One represents the rays after an even number of reflections, the other represents the rays after an odd number of reflections. These are

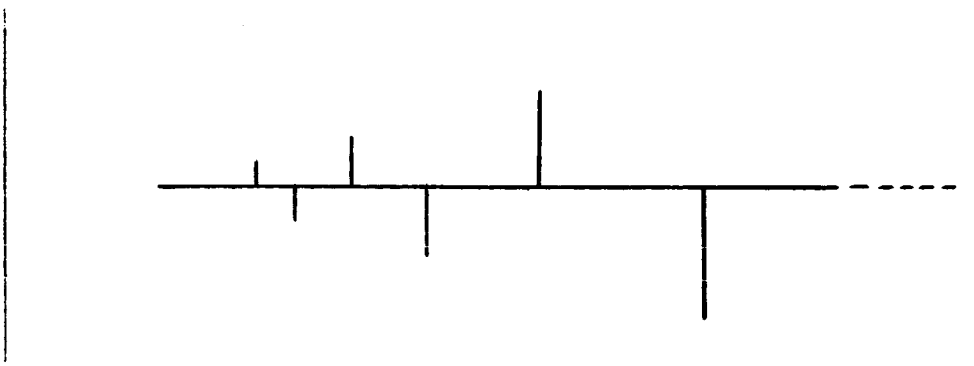

(a) Top View

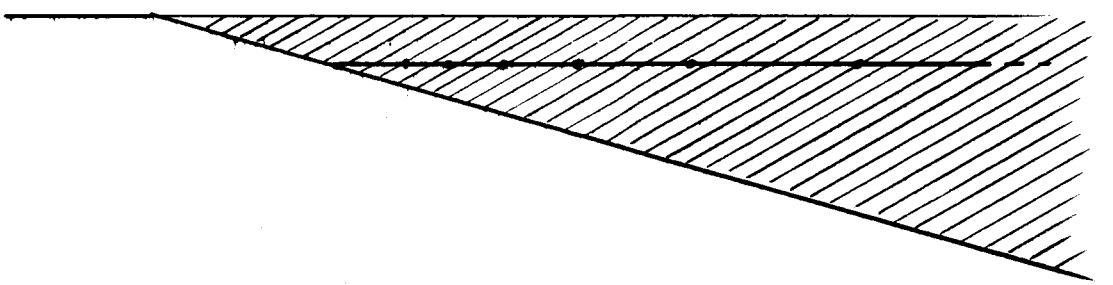

(b) Side View

Figure 6. The structure of log periodic monopole antenna in a dielectric medium.

expressed in Figure 7 as the group of k_2, k_3, k_4, ... images and the group of k_1', k_2', k_3', ... images.

From the geometrical construction of Figure 7, we get the following relations:

$$R_K = \sqrt{(S_k + d \cot \gamma)^2 + d^2} \tag{15}$$

$$\theta_{k_1} = -\sin^{-1} \frac{d}{R_k} \tag{16}$$

$$\theta_{kh} = \theta_{kl} - 2\gamma(h-1) \tag{17}$$

$$\theta'_{kh} = -\theta_{kl} - 2\gamma h \tag{18}$$

$$R_{kh} = R_k (\cos \theta_{kh} - \sin \theta_{kh} \cot \phi) \tag{19}$$

$$R'_{kh} = R_k (\cos \theta'_{kh} - \sin \theta'_{kh} \cot \phi) \tag{20}$$

$$d_{kh} = - R_k \sin \theta_{kh} \csc \phi \tag{21}$$

$$d'_{kh} = - R_k \sin \theta'_{kh} \csc \phi \tag{22}$$

The Kth element carries current I_k. If there is no reflection or refraction, the relation between the electrical field and the current is (in the H-plane)

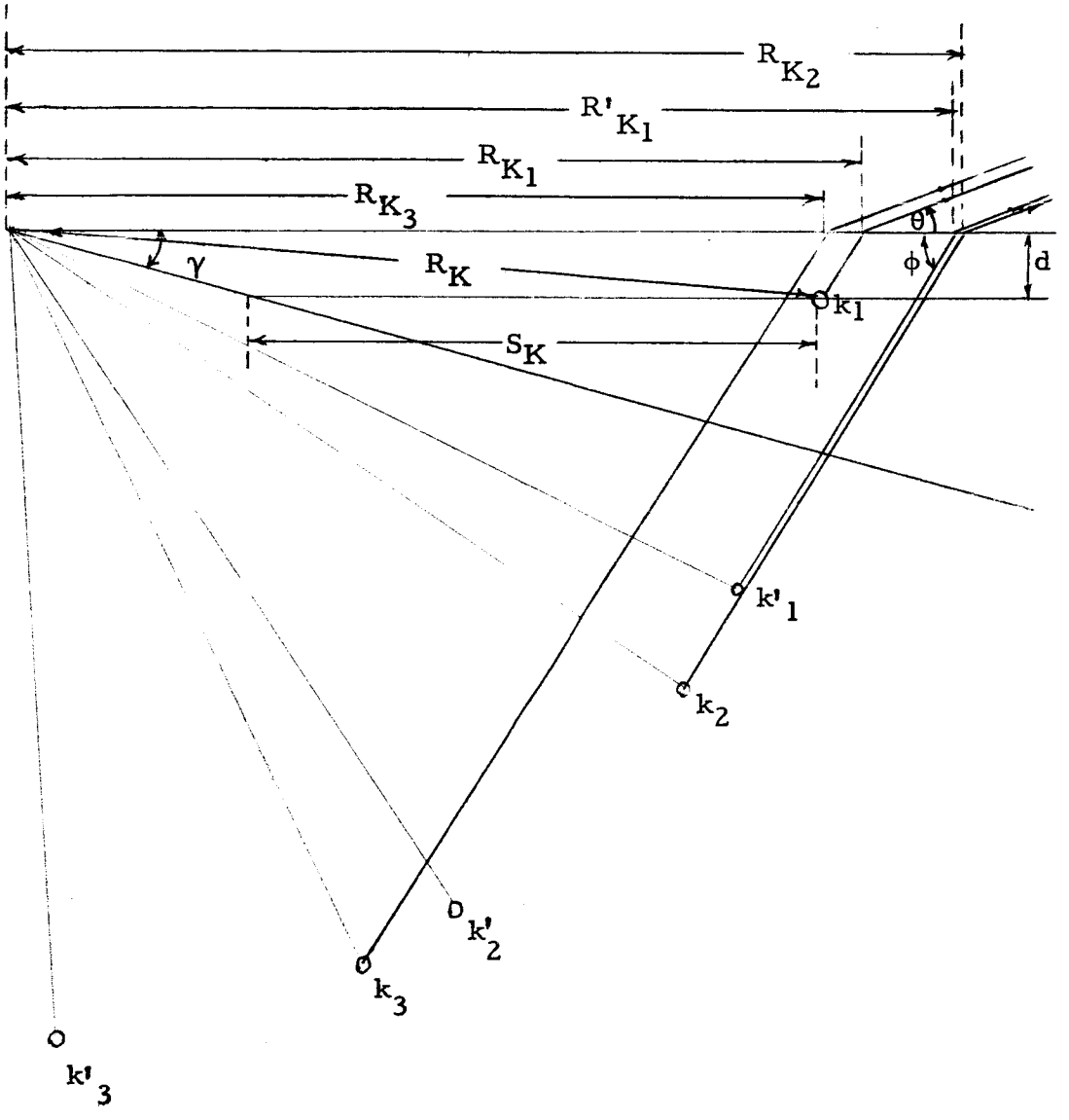

Figure 7. The image diagram of one element in a dielectric medium.

$$E_k = C_k I_k e^{-j(\beta_d S_k + \theta_k)} \tag{23}$$

where θ_k = The phase angle of the self impedance of the Kth element.

$-\beta_d S_k$ = The phase angle of the applied voltage on the terminal of the Kth element.

The factor C_k varies with l_k, the relation is [2]

$$C_k = \frac{1 - \cos \beta_d L_k}{\sin \beta_d L_k} \tag{24}$$

The radiation field due to the images are

$$E_{kh} = a\, b^{h-1} E_k e^{-j\beta_d d_{kh}} \tag{25}$$

$$E'_{kh} = -a\, b^{h-1} E_k e^{-j\beta_d d'_{kh}} \tag{26}$$

Where a is the refraction factor from dielectric medium to air, and b is the reflection factor in the boundary of the dielectric medium and air, the values are [2]

$$a = \left| 1 + \frac{\sin\phi - \sqrt{\frac{1}{\epsilon_r} - \cos^2\phi}}{\sin\phi + \sqrt{\frac{1}{\epsilon_r} - \cos^2\phi}} \right| \tag{27}$$

$$b = \left| \frac{\sin\phi - \sqrt{\frac{1}{\epsilon_r} - \cos^2\phi}}{\sin\phi + \sqrt{\frac{1}{\epsilon_r} - \cos^2\phi}} \right| \tag{28}$$

Shown in Figure 7 is the boundary of the dielectric medium. Only those rays, from any image source, which go through the limited dielectric surface will actually radiate power externally. Rays in other directions will be assumed to be unimportant. Thus, the limiting angle of radiation are different with each element and its images.

Assume ϕ_{kh} and ϕ'_{kh} are the limited angles for the elements as Figure 7 showed, then we got

$$\phi_{kh} = \pi + \theta_{kh} \tag{29}$$

$$\phi'_{kh} = \pi + \theta'_{kh} \tag{30}$$

It is necessary to use the unit function [3] to satisfy the boundary conditions. This is also convenient for computer programming. The total field of the kth element is then

$$\begin{aligned}(E_k)_{total} = &\sum_{h=1}^{n} a b^{h-1} C_h I_k e^{-j[\beta_0(d_{kh}+S_k)+\beta(r_0-R_{kh}\cos\theta)+\theta_k]} u(\phi_{kh}-\phi) \\ &- \sum_{h=1}^{n'} a b^{h-1} C_h I_k e^{-j[\beta_0(d'_{kh}+S_k)+\beta(r_0-R'_{kh}\cos\theta)+\theta_k]} u(\phi'_{kh}-\phi)\end{aligned} \tag{31}$$

where n and n' are the maximum values of h for the limits ϕ_{kh} and ϕ'_{kh}.

Taking the summation over all elements gives the total field of the entire antenna

$$E_{total} = \sum_{k=0}^{\infty} (-1)^k \left[\sum_{k=1}^{n} a b^{k-1} C_k I_k e^{-j[\beta_k (d_{kk} + S_k) + \beta (r_0 - R_{kk} \cos\theta) + \theta_k]} u(\phi_{kk} - \phi) \right.$$

$$\left. - \sum_{k=1}^{n'} a b^{k-1} C_k I_k e^{-j[\beta_k (d'_{kk} + S_k) + \beta (r_0 - R'_{kk} \cos\theta) + \theta_k]} u(\phi'_{kk} - \phi) \right] \tag{32}$$

The theoretical and experimental patterns of this type antenna in different dielectric mediums are plotted on Figure 8.

In Figure 9 the limits of calculation are shown. The region of β' is excluded for reasons shown in the second section. In the β angle region, the theoretical pattern does not agree with the expreimental pattern, even though it is theoretically correct. The larger dielectric constant material cuases the pattern to be depressed a larger amount than the $\epsilon_r = 2.25$ material. The reduction of power in the β angle region on the experimental pattern, is possibly due to the influence of the edge of the dielectric cover. To explain this, note that part of the energy emerges in the direction shown by the ray marked a while other energy to the same distant point could emerge along the ray marked b. The total power in this direction is the sum of a and b. These rays could be out of phase resulting in cancellation of the field. The limit of the β angle region is determined by the length, thickness and dielectric constant of the covering layer.

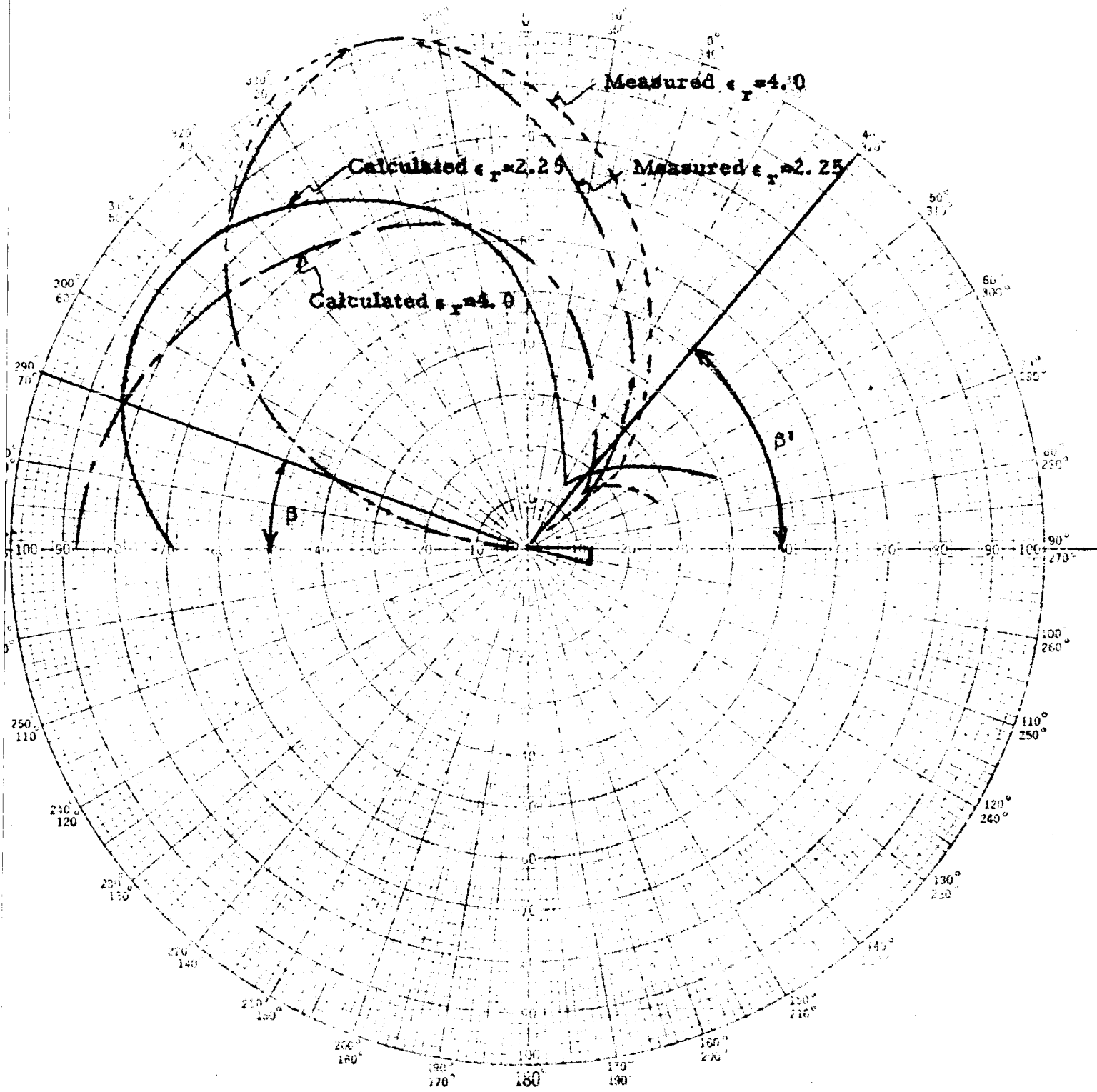

Figure 8. H-plane patterns, ϵ_r = 2.25 and ϵ_r = 4.0.

Polar Chart No. 127

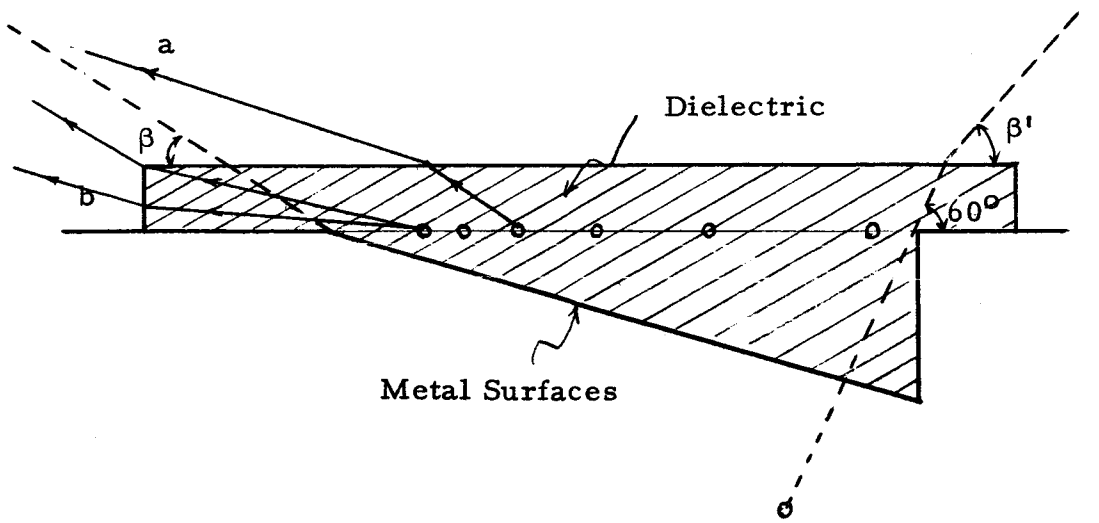

Figure 9. Construction of the dielectric filled cavity.

CONCLUSION

The impedance distribution of elements is such that, the resonant element has the lowest impedance and the impedance of the other elements increase with their separation from the resonant element. The current in the element reduces as the impedance rises. In these models, four elements are assumed to be in the active region. As the logarithmic parameter τ is increased, more elements become active and the antenna gain is increased.

For an actual log periodic monopole antenna, the frequency range of variation is dependent upon the number of elements. The more elements, the wider the frequency range which can be used. If more elements are used, an increase in the length of the center feed line is necessary thus permitting variation in potential along the feed line and a consequent deviation from the assumption of constant voltage described above.

In summary, this study has shown that the method of images applied to a log periodic antenna over a reflecting sheet yields a reasonably precise theoretical determination of the radiation pattern of the structure, less precise in the dielectric case, but still reasonably useful. The method is laborious and is best suited to the use of the computer. The presence of a dielectric in the structure

complicates the problem because of images across the dielectric-air boundary.

The final conclusion is that the calculations of complicated strucutres may serve as a guide to performance but cannot replace measured performance.

APPENDIX

CALCULATION OF THE THREE DIMENSIONAL RADIATION FIELD OF A LOG PERIODIC ANTENNA

The Radiation Pattern of One Element

The current distribution on the kth element is assumed as

$$I_k(y) = (I_k)_m \sin \beta(L_k - |y|) \tag{32}$$

After we put the antenna in a coordinate system, there are some elements in the +y region, some elements in the -y region. The calculation of the two cases are different. They will be discussed separately.

Case 1: The elements in the +y region:

The current distribution on the kth element is

$$I_k(y) = (I_k)_m \sin \beta(L_k - y) \tag{33}$$

As shown in the far field vector potential due to a small current segment $I_k(y)dy$ is

$$\vec{dA}_k = \frac{I_k(y)dy}{4\pi r_o} e^{-j\beta(r_o - \vec{P}_k \cdot (\vec{r}_o/r_o) - \vec{u} \cdot (\vec{r}_o/r_o)} \tag{34}$$

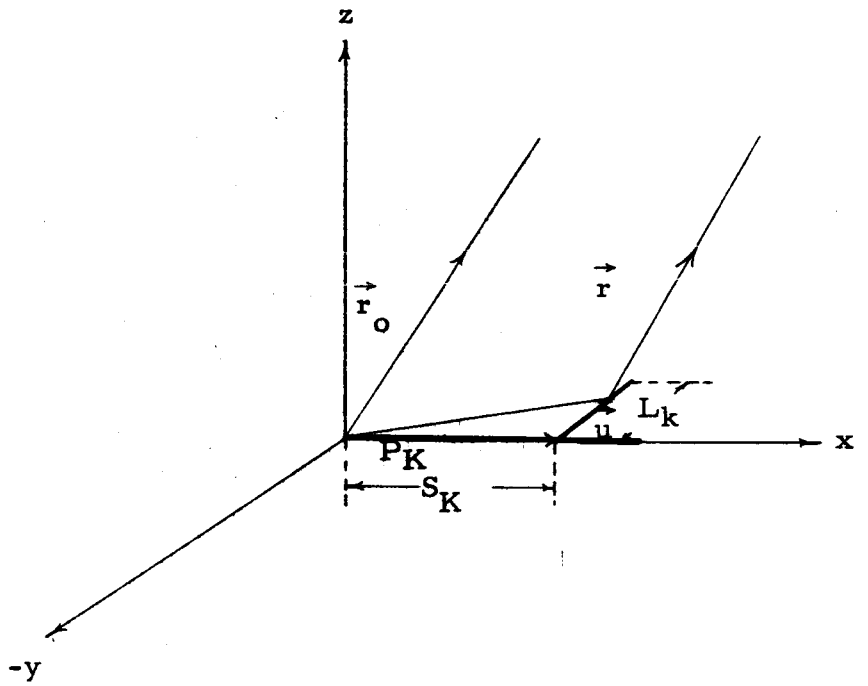

Figure 10. The coordinate system for one element.

where $\vec{u} = (0, y, o)$

$\vec{P}_k = (S_k, 0, 0)$

$\vec{r}_o/r_o = (\sin\theta\cos\phi, \sin\theta\sin\phi, \cos\theta)$

Combining Equations (33) and (34), the result is:

$$dA_k = \frac{(I_k)_m \sin\beta(L_k - y)}{4\pi r_o} e^{-j\beta(r_o - S_k \sin\theta\cos\phi - y\sin\theta\sin\phi)} dy \tag{35}$$

Taking the integral over the whole antenna gives

$$A_k = \frac{(I_k)_m}{4\pi r_o} e^{-j\beta(r_o - S_k\sin\theta\cos\phi)} \left[\sin\beta l_k \int_o^{l_k} \cos\beta y\, e^{j\beta y\sin\theta\sin\phi} dy - \cos\beta l_k \int_o^{l_k} \sin\beta y\, e^{j\beta y\sin\theta\sin\phi} dy\right] \tag{36}$$

By No. 430 and No. 431 of Pierce's Tables of Integrals

$$\int e^{ax} \sin px\,dx = \frac{e^{ax}(a\sin px - p\cos px)}{a^2 + p^2}$$

$$\int e^{ax} \cos px\,dx = \frac{e^{ax}(a\cos px + p\sin px)}{a^2 + p^2}$$

The result of Equation (36) then becomes

$$A_k = \frac{(I_k)_m}{4\pi r_o \beta(1 - \sin^2\theta\sin^2\phi)} e^{-j\beta(r_o - S_k\sin\theta\cos\phi)} \left[e^{j\beta L_k \sin\theta\sin\phi} - \cos\beta L_k - j\sin\theta\sin\phi\sin\beta L_k\right] \tag{37}$$

The three components in space are

$$\left.\begin{aligned} (A_k)_x &= 0 \\ (A_k)_y &= \frac{(I_k)_m e^{-j\beta(r_0 - S_k \sin\theta\cos\phi)}}{4\pi r_0 \beta(1-\sin^2\theta\sin^2\phi)}\left[e^{j\beta l_k \sin\theta\sin\phi} - \cos\beta l_k - j\sin\theta\sin\phi\sin\beta l_k\right] \\ (A_k)_z &= 0 \end{aligned}\right\} \quad (38)$$

Case 2: The elements in the -y region:

The current distribution becomes

$$I_k(y) = (I_k)_m \sin\beta(L_k + y) \quad (39)$$

By the same method, the result is

$$\left.\begin{aligned} (A_k)_x &= 0 \\ (A_k)_y &= -\frac{(I_k)_m e^{-j\beta(r_0 - S_k \sin\theta\cos\phi)}}{4\pi r_0 \beta(1-\sin^2\theta\sin^2\phi)}\left[e^{-j\beta l_k \sin\theta\sin\phi} - \cos\beta l_k + j\sin\theta\sin\phi\sin\beta l_k\right] \\ (A_k)_z &= 0 \end{aligned}\right\} \quad (40)$$

If we assume the nth element is placed in the +y region, then we can write a general equation which includes both cases, that is

$$(A_k)_y = \frac{(I_k)_m e^{-j\beta(r_0 - S_k \sin\theta\cos\phi)}}{4\pi r_0 \beta(1-\sin^2\theta\sin^2\phi)}\left[(-1)^{n-k}\left\{e^{j(-1)^{n-k}\beta(l_k \sin\theta\sin\phi)} - \cos\beta l_k\right\} - j\sin\theta\sin\phi\sin\beta l_k\right] \quad (41)$$

If the nth element is the resonant element $L_n \cong \frac{\lambda}{4}$, by Equation (2) and Equation (1), the values of L_k, and S_k are

$$L_k = \tau^{n-k} \frac{\lambda}{4} \tag{42}$$

$$S_k = \tau^{n-k} \frac{\lambda}{4} \cot \alpha \tag{43}$$

Substituting Equation (42) and Equation (43) into Equation (41), the result is

$$(A_k)_y = \frac{e^{-j\beta r_0}}{4\pi r_0 \beta (1 - \sin^2\theta \sin^2\phi)} (I_k)_m \, e^{j\frac{\pi}{2}\tau^{n-k} \cot\alpha \sin\theta \cos\phi} \cdot \left[(-1)^{n-k} e^{j(-\tau)^{n-k} \frac{\pi}{2} \sin\theta \sin\phi} - (-1)^{n-k} \cos\left(\frac{\pi}{2}\tau^{n-k}\right) - j \sin\theta \sin\phi \sin\left(\frac{\pi}{2}\tau^{n-k}\right) \right] \tag{44}$$

The Radiation Pattern of the Entire Antenna

Taking the summation of all elements, the total vector potential in the y direction is

$$A_y = \frac{e^{-j\beta r_0}}{4\pi r_0 \beta (1 - \sin^2\theta \sin^2\phi)} \sum_{k=0}^{\infty} (I_k)_m \, e^{j\frac{\pi}{2}\tau^{n-k} \cot\alpha \sin\theta \cos\phi} \cdot \left[(-1)^{n-k} e^{j(-\tau)^{n-k} \frac{\pi}{2} \sin\theta \sin\phi} - (-1)^{n-k} \cos\left(\frac{\pi}{2}\tau^{n-k}\right) - j \sin\theta \sin\phi \sin\left(\frac{\pi}{2}\tau^{n-k}\right) \right] \tag{45}$$

Equation (45) is the vector potential due to the actual elements. The vector potential due to the images can be caluclated using a similar method, with the elements redistributed on an inclined plane. The

result obtained is

$$A_y' = \frac{-e^{-j\beta r_0}}{4\pi r_0 \beta (1-\sin^2\theta \sin^2\phi)} \sum_{k=0}^{\infty} (I_k)_m \, e^{j\frac{\pi}{2}\tau^{n-k}(\cos\gamma \sin\theta\cos\phi - \sin\gamma\cos\theta)} \cdot$$

$$\left[(-1)^{n-k} e^{j\frac{\pi}{2}(-\tau)^{n-k}\sin\theta\sin\phi} - (-1)^{n-k}\cos\left(\frac{\pi}{2}\tau^{n-k}\right) - j\sin\theta\sin\phi\,\sin\left(\frac{\pi}{2}\tau^{n-k}\right)\right] \tag{46}$$

The sum of the electric fields due to the actual elements and their images is the total field. This is

$$(A_y)_{total} = \frac{e^{-j\beta r_0}}{4\pi r_0 \beta (1-\sin^2\theta\sin^2\phi)} \sum_{k=0}^{\infty} (I_k)_m \left[e^{j\frac{\pi}{2}\tau^{n-k}\cot\alpha\sin\theta\cos\phi} - e^{j\frac{\pi}{2}\tau^{n-k}(\cos\gamma\sin\theta\cos\phi - \sin\gamma\cos\theta)\cot\alpha}\right] \cdot$$

$$\left[(-1)^{n-k} e^{j(-\tau)^{n-k}\frac{\pi}{2}\sin\theta\sin\phi} - (-1)^{n-k}\cos\left(\frac{\pi}{2}\tau^{n-k}\right) - j\sin\theta\sin\phi\,\sin\left(\frac{\pi}{2}\tau^{n-k}\right)\right] \tag{47}$$

From Equations (4) and (5), the maximum current in the kth element is

$$(I_k)_m = \frac{V\, e^{-j(\frac{\pi}{2}\tau^{n-k}\cot\alpha + \theta_k)}}{A_k \sin(\frac{\pi}{2}\tau^{n-k})} \tag{48}$$

where V is the value of applied voltage, Z_k and θ_k are the magnitude and phase angle of the impedance of the Kth element, which can be found from an impedance characteristic curve.

Transfer the electric field in the y direction into spherical coordinate by the relations

$$A_\theta = A_y \sin\phi \cos\theta \tag{49}$$

$$A_\phi = A_y \cos\phi \tag{50}$$

The relation between the field strength and vector potential is

$$\vec{E} = -j\omega\mu_o \vec{A} \tag{51}$$

Then the θ and ϕ components of electrical field are

$$E_\theta(\theta,\phi,\alpha,\gamma,\tau) = \frac{j\omega\mu_o V e^{-j\beta r_o}}{4\pi r_o \beta} F_\theta(\theta,\phi,\alpha,\gamma,\tau) \tag{52}$$

$$E_\phi(\theta,\phi,\alpha,\gamma,\tau) = \frac{j\omega\mu_o V e^{-j\beta r_o}}{4\pi r_o \beta} F_\phi(\theta,\phi,\alpha,\gamma,\tau) \tag{53}$$

where

$$F_\theta(\theta,\phi,\alpha,\gamma,\tau) = \frac{\cos\theta \sin\phi}{(1-\sin^2\theta\sin^2\phi)} \sum_{k=0}^{\infty} \frac{e^{-j\left(\frac{\pi}{2}\tau^{n-k}\cot\alpha + \theta_k\right)}}{Z_k \sin\left(\frac{\pi}{2}\tau^{n-k}\right)} \cdot$$

$$\left[e^{j\frac{\pi}{2}\tau^{n-k}\cot\alpha \sin\theta\cos\phi} - e^{j\frac{\pi}{2}\tau^{n-k}(\cos 2\gamma \sin\theta\cos\phi - \sin 2\gamma\cos\theta)\cot\alpha}\right] \cdot \tag{54}$$

$$\left[(-1)^{n-k} e^{j(-\tau)^{n-k}\frac{\pi}{2}\sin\theta\sin\phi} - (-1)^{n-k}\cos\left(\frac{\pi}{2}\tau^{n-k}\right) - j\sin\theta\sin\phi\sin\left(\frac{\pi}{2}\tau^{n-k}\right)\right]$$

$$F_\phi(\theta,\phi,\alpha,\gamma,\tau) = \frac{\cos\phi}{(1-\sin^2\theta\sin^2\phi)} \sum_{k=0}^{\infty} \frac{e^{-j\left(\frac{\pi}{2}\tau^{n-k}\cot\alpha + \theta_k\right)}}{Z_k \sin\left(\frac{\pi}{2}\tau^{n-k}\right)} \cdot$$

$$\left[e^{j\frac{\pi}{2}\tau^{n-k}\cot\alpha \sin\theta\cos\phi} - e^{j\frac{\pi}{2}\tau^{n-k}(\cos 2\gamma \sin\theta\cos\phi - \sin 2\gamma\cos\theta)\cot\alpha}\right] \cdot \tag{55}$$

$$\left[(-1)^{n-k} e^{j(-\tau)^{n-k}\frac{\pi}{2}\sin\theta\sin\phi} - (-1)^{n-k}\cos\left(\frac{\pi}{2}\tau^{n-k}\right) - j\sin\theta\sin\phi\sin\left(\frac{\pi}{2}\tau^{n-k}\right)\right]$$

These are the final resulting equations of the three dimensional pattern.

REFERENCES

[1] Clark, C., W. L. Jones, and A. Leigh, 1962 "A Theoretical and Experimental Investigation of Flush Mounting Configurations for Log Periodic Structures," Utah State University, Engineering Experiment Station Report.

[2] Jordan, Edward C., 1955 Electromagnetic Waves and Radiating System, Prentice-Hall Book Company, Electrical Engineering Series.

[3] C. R. Wylie, 1960 Advanced Engineering Mathematics, McGraw-Hill Book Co., Inc., New York, N. Y.

[4] Isbell, D. E., 1960, "Log Periodic Dipole Arrays," IRE Trans. Vol. Ap-8, pp 260-267, May.

[5] Whale, Richard L., and C. Clark, 1963, "A Log Periodic Monopole Antenna in a Dielectric Field Cavity," Utah State University, Engineering Experiment Station Report.